NAVAL
POSTGRADUATE
SCHOOL

MONTEREY, CALIFORNIA

THESIS

EFFECTS OF RADIO WAVE PROPAGATION IN URBANIZED AREAS ON UAV-GCS COMMAND AND CONTROL

by

Lock Wai Lek Willy

December 2003

Thesis Advisor:	David C. Jenn
Second Reader:	Jeffery B. Knorr

Approved for public release, distribution is unlimited

THIS PAGE INTENTIONALLY LEFT BLANK

REPORT DOCUMENTATION PAGE			Form Approved OMB No. 0704-0188
Public reporting burden for this collection of information is estimated to average 1 hour per response, including the time for reviewing instruction, searching existing data sources, gathering and maintaining the data needed, and completing and reviewing the collection of information. Send comments regarding this burden estimate or any other aspect of this collection of information, including suggestions for reducing this burden, to Washington headquarters Services, Directorate for Information Operations and Reports, 1215 Jefferson Davis Highway, Suite 1204, Arlington, VA 22202-4302, and to the Office of Management and Budget, Paperwork Reduction Project (0704-0188) Washington DC 20503.			
1. AGENCY USE ONLY ***(Leave blank)***	**2. REPORT DATE** December 2003	**3. REPORT TYPE AND DATES COVERED** Master's Thesis	
4. TITLE AND SUBTITLE: Title (Mix case letters) Effects of Radio Wave Propagation in Urbanized Areas On UAV-GCS Command and Control			**5. FUNDING NUMBERS**
6. AUTHOR(S) Lock Wai Lek Willy			
7. PERFORMING ORGANIZATION NAME(S) AND ADDRESS(ES) Naval Postgraduate School Monterey, CA 93943-5000			**8. PERFORMING ORGANIZATION REPORT NUMBER**
9. SPONSORING /MONITORING AGENCY NAME(S) AND ADDRESS(ES) N/A			**10. SPONSORING/MONITORING AGENCY REPORT NUMBER**
11. SUPPLEMENTARY NOTES The views expressed in this thesis are those of the author and do not reflect the official policy or position of the Department of Defense or the U.S. Government.			
12a. DISTRIBUTION / AVAILABILITY STATEMENT Approved for public release, distribution is unlimited			**12b. DISTRIBUTION CODE**

13. ABSTRACT *(maximum 200 words)*

The purpose of this research was to examine the effects of radiowave propagation in urbanized areas on unmanned aerial vehicle-ground control station (UAV-GCS) command and control.

Operating at high frequency has merits of higher data rate transfer, which is crucial to support the large quantity of voice and video data to be transmitted via UAV-GCS linkage. However, high frequencies are attenuated more rapidly in lossy materials and weather. Having a shorter operational range translates to a smaller RF spread radius, and thus lowers the susceptibility to detection and jamming.

The software, Urbana, was used to investigate the propagation of radio signals in urban environments under varying conditions. Simulations were conducted for a small group of buildings and a large collection of buildings representative of a big city. The data clearly illustrate the effect of "urban canyons" and diffraction around buildings.

An UAV deployed for military operations in urban terrain (MOUT) must have the inherent capability to hover or fly at low speeds to be able to adapt to the dynamic urban environment and to capitalize on communications opportunities. Simulations show that a single UAV hovering at three times the height of the tallest building in the central city was found to provide concentric, uniform signal coverage.

14. SUBJECT TERMS Unmanned aerial vehicles, Urbana wireless toolset, Propagation models, Airborne communications node, Portable ground control system			**15. NUMBER OF PAGES** 107 **16. PRICE CODE**
17. SECURITY CLASSIFICATION OF REPORT Unclassified	**18. SECURITY CLASSIFICATION OF THIS PAGE** Unclassified	**19. SECURITY CLASSIFICATION OF ABSTRACT** Unclassified	**20. LIMITATION OF ABSTRACT** UL

NSN 7540-01-280-5500 Standard Form 298 (Rev. 2-89)
Prescribed by ANSI Std. 239-18

THIS PAGE INTENTIONALLY LEFT BLANK

Approved for public release, distribution is unlimited

EFFECTS OF RADIO WAVE PROPAGATION IN URBANIZED AREAS ON UAV-GCS COMMAND AND CONTROL

Lock Wai Lek Willy
Major, Singapore Armed Forces (Army)
B.Eng., National Defense Academy, Japan, 1998

Submitted in partial fulfillment of the
requirements for the degree of

MASTER OF SCIENCE IN ELECTRICAL ENGINEERING

from the

NAVAL POSTGRADUATE SCHOOL
December 2003

Author: Lock Wai Lek Willy

Approved by: David C. Jenn
Thesis Advisor

Jeffrey B. Knorr
Second Reader

John P. Powers
Chairman, Department of Electrical and Computer Engineering

THIS PAGE INTENTIONALLY LEFT BLANK

ABSTRACT

The purpose of this research was to examine the effects of radiowave propagation in urbanized areas on unmanned aerial vehicle-ground control station (UAV-GCS) command and control.

Operating at high frequency has merits of higher data rate transfer, which is crucial to support the large quantity of voice and video data to be transmitted via UAV-GCS linkage. However, high frequencies are attenuated more rapidly in lossy materials and weather. Having a shorter operational range translates to a smaller RF spread radius, and thus lowers the susceptibility to detection and jamming.

The software, Urbana, was used to investigate the propagation of radio signals in urban environments under varying conditions. Simulations were conducted for a small group of buildings and a large collection of buildings representative of a big city. The data clearly illustrate the effect of "urban canyons" and diffraction around buildings.

An UAV deployed for military operations in urban terrain (MOUT) must have the inherent capability to hover or fly at low speeds to be able to adapt to the dynamic urban environment and to capitalize on communications opportunities. Simulations show that a single UAV hovering at three times the height of the tallest building in the central city was found to provide concentric, uniform signal coverage.

THIS PAGE INTENTIONALLY LEFT BLANK

TABLE OF CONTENTS

LIST OF FIGURES

LIST OF TABLES

THIS PAGE INTENTIONALLY LEFT BLANK

ACKNOWLEDGMENTS

I would like to express my most sincere gratitude to Professor David Jenn of the Naval Postgraduate School, Monterey, California for his guidance and invaluable contributions to the completion of this work. He has never failed to stop whatever work he is doing to attend to my questions and I really appreciate it. I would also like to thank Professor Jeffrey Knorr for agreeing to be the second reader to the thesis. Both of them have prepared me in antenna theory, microwave engineering and radar cross section theory while I was in Naval Postgraduate School and the knowledge acquired has allowed me to proceed with the thesis work.

THIS PAGE INTENTIONALLY LEFT BLANK

EXECUTIVE SUMMARY

In military applications, unmanned aerial vehicles (UAVs) can contribute significantly to the war fighting capability of the operational forces by the information collected. Data collected first-hand from the battlefield are not only accurate, but can be processed rapidly to assist commanders in maneuvering the troops. When reconnaissance, intelligence, surveillance, and target acquisition are the premier missions, substantial information pertaining to intelligence preparation of the battlefield, situation development, battle management, battle damage assessment and rear area security can also be collected by UAVs.

The mechanisms that govern radiowave propagation in outdoor urbanized areas are complicated, but they can generally be attributed to three basic propagation methods: (1) reflection, (2) diffraction, and (3) scattering. As a result of these three propagation mechanisms, the received signal strength at the ground control stations (GCS) can be roughly characterized by three nearly independent phenomena of large-scale path loss, large-scale shadowing and multipath fading. UAV-to-GCS command links in urban environments are subject to severe degradation due to the superposition of the three mechanisms. Severe multipath can result in a complete loss of command signals, which can limit the operational area or even cause a loss of the vehicle.

The purpose of this research was to examine the effects of urbanized areas on the propagation of radio waves. This, in turn, affects the linkage between a UAV and its ground control station. The **Urbana** wireless toolset provided a means to predict multipath signals of wireless networks in complex urban environments.

Several computer-aided design (CAD) models representative of multiple rooms, suburban intersections, and central city areas were initially built using **Cifer**. Several scenarios were developed to approximate the propagation of electromagnetic waves in the models. These scenarios included flying UAVs across the city and changing parameters such as altitude, frequency, phase of signal transmissions on two separate UAVs, and number and positioning of UAVs. Indoor reception of GCS signals in varying designs of rooms, and building materials was also simulated. Each simulation included the effects of polarization, diffraction effects, antenna patterns, and transmitting power.

The simulation results indicate that there exists an optimal operating altitude of a UAV for signal coverage. Perching at rooftops to minimize power consumption may not be ideal, as most of the radio frequency (RF) waves will simply be reflected upwards. If the UAV is positioned too high above buildings, the areas beneath the UAV will experience a null when using a vertical monopole antenna and, thus, the power received by the GCS will be diminished. A single UAV operating at three times the height of the tallest building in the central city was found to provide a concentric, uniform signal coverage.

The research also found that signal contours within a house are affected by the height of the UAV, thickness of walls, location of openings, and the indoor arrangement. Diffraction from the edges of surrounding buildings allows propagation of radio waves into the house without direct line of sight between the UAV and GCS. Simulation results show that areas away from the windows may have a higher signal strength level than at the windows due to multipath interference.

In summary, the effects of radiowave propagation in urbanized areas are determining factors to the deployment of the UAV and GCS to obtain ideal signal linkage. Deploying UAVs as airborne communications nodes improves signal coverage. By understanding the propagation effects and from analyzing signal contours, planners for MOUT will be able to provide continuous, uninterrupted and constant signal linkage between assaulting elements (troops and artillery) and supporting elements (sensors and logistics).

I. INTRODUCTION

A. UNMANNED AERIAL VEHICLE

Many armed forces around the world, like the United States Armed Forces and the Singapore Armed Forces (SAF), have long recognized the tremendous potential of unmanned aerial vehicles (UAVs) for battlefield surveillance and reconnaissance. The UAV is particularly suitable for the SAF because it is less manpower intensive than human intelligence. Casualties will also be reduced, which is especially important for Singapore as the bulk of the SAF is made of conscript soldiers and reservists. By and large, SAF is constantly exploring new technologies that might be applied to its unique requirements.

UAVs are remotely piloted or self-piloted aircraft that can carry cameras, sensors, communications equipment or other payloads. They have been used in reconnaissance and intelligence gathering roles since the 1950s and more challenging roles like combat missions are envisioned. UAVs are generally categorized by range, altitude and flight durations.

During peacetime, UAVs can be used to monitor traffic situations on the roads, guard coastal areas against probable hostile or illegal infiltrations or locate vessels that have sent out distress signals. In the civilian arenas, the potential applications of UAVs are numerous. They are exceptionally useful for deployment in hazardous areas. Using them instead of humans will greatly reduce any chance of human casualties. Apart from these applications, they can also be used for oil exploration, or in agricultural fields to help in spraying of insecticide.

In military applications, UAVs can contribute significantly to the war fighting capability of the operational forces by the information collected. Data collected first-hand from the battlefield are not only accurate but can be processed rapidly to assist commanders in troop maneuvers. When reconnaissance, intelligence, surveillance, and target acquisition are the premier missions, substantial information pertaining to

intelligence preparation of the battlefield, situation development, battle management, battle damage assessment and rear area security can also be collected by UAVs, as depicted in Figure 1.

(a) (b)

Figure 1. (a) Troops deploying UAVs for reconnaissance. (b) UAVs deployed on rooftop to maintain surveillance and signal relay (From Ref. [1].).

They can also be used as drones for training aircraft pilots and weapon systems, and as a total replacement of manned attack aircraft. The latter application, as an unmanned combat air vehicle (UCAV), is still in the research and development phase. Examples are the efforts by Boeing and Northrop Grumman, each having an experimental aircraft, X-45 and X-47, respectively. The United States Central Intelligence Agency's air strike against Al-Qaeda operatives in Yemen in November 2002 demonstrated the UAV's transition from a surveillance drone to a hunter-killer asset. The mission saw a RQ-1 Predator, developed by General Atomics Aeronautical Systems, destroy a vehicle by launching an AGM-114 Hellfire air-to-surface missile.

A UCAV can be employed either as an independent system or in conjunction with other airborne, ground-based, and space-based systems. One version can be designed to loiter at high altitude over the region of interest for long periods of time (>24 hours) until called upon to strike a target. In its subsonic loiter mode it would be able to perform a surveillance and reconnaissance mission. An example would be RQ-4 Global Hawk jointly developed by Northrop Grumman and Raytheon, which is capable of standoff, sustained high altitude surveillance and reconnaissance. It will operate at ranges up to 3000 nautical miles from its launch area, with loiter capability over the target area of up

to 24 hours at altitudes greater than 60,000 feet. It will be capable of simultaneously carrying electro-optical (EO), infrared (IR), and synthetic aperture radar (SAR) payloads, and will also be capable of both wideband satellite and line-of-sight (LOS) data link communications.

It could also be used as part of a bistatic configuration in which a region of interest would be assessed in real-time while the related information would be received and processed by a different sensor. As a secondary mission, it could also be made to perform electronic countermeasures (ECM) and electronic counter-countermeasures (ECCM) roles.

B. PROPAGATION ISSUES

The mechanisms, which govern radio propagation in outdoor urbanized areas, are complicated, but they can be generally be attributed to three basic propagation methods: (1) reflection, (2) diffraction, and (3) scattering [2]. As a result of these three propagation mechanisms, the received signal strength at the ground control station (GCS) can be roughly characterized by three nearly independent phenomena of large-scale path loss, large scale shadowing, and multipath fading. UAV-GCS command links in urban environments are subjected to severe degradation due to the superposition of the three mechanisms.

Existing data links for UAVs are point-to-point communication links between the UAV and a GCS. However, future concept of operations (CONOPS) would involve UAV or payload control from soldiers in units other than the controlling units. These operations require future systems to evolve from control center to network centric application. UAV command, control and data links experience a unique propagation environment when operating in urban areas. Severe multipath can result in a complete loss of command signals, which can limit the operational area or even cause a loss of the vehicle. Common frequency bands used by existing UAVs include C and Ku band for LOS data links and Ku band for beyond line-of-sight satellite data links.

For example, the Pioneer system utilizes a jam-resistant, direct sequence spread spectrum uplink command channel at C band. The video and telemetry downlink, also at C band, utilizes a state-of-the-art high power solid-state amplifier and directional antennas on both the tracking control unit and air vehicle, assuring excellent quality video for the commander in the field. An omni-directional UHF backup link is provided for redundancy in this key subsystem.

A typical UAV GCS is a 30 by 8 by 8 foot, triple-axle, commercially available trailer. The trailer incorporates an integral uninterrupted power supply (UPS); environmental control system (cooling only); pilot and payload operator (PPO) workstations; data exploitation, mission planning, communication (DEMPC) terminals; and SAR workstations. All mission imagery recording is located in the GCS. System power is supplied either by commercial hook ups or by dual external 35-kW generators.

C. PREVIOUS RESEARCH

Over the past fifteen years, there has been extensive investigation of the propagation of electromagnetic waves in urban terrain, mostly motivated by the growth of commercial wireless systems. Walfisch and Bertoni [3,4] modeled the rows of city buildings as a series of absorbing diffracting screens of uniform height. The forward diffraction, along the screens, with a final diffraction down to the street level gave an overall propagation model for the case of an elevated fixed antenna above the roofline to a location at street level.

In Reference [5], experiments and modeling studies of the indoor radio channel multipath characteristics and their effect on transmit and receive ranges are presented. The paper concludes that the indoor multipath varies considerably depending upon the building dimension, transmit/receive range, interior layout, and furnishings.

Reference [6] compares indoor narrowband and wideband measurements to ray tracing using geometrical optics (GO) and the geometrical theory of diffraction (GTD) methods. The results indicate that ray-tracing techniques based on full three-dimensional

implementations could provide an accurate characterization of the outdoor propagation problem.

D. OBJECTIVE AND TECHNICAL APPROACH

The purpose of this research is to examine the effects of radio wave propagation in urbanized areas on UAV-GCS command and control.

The **Urbana** Toolset offers a solution for predicting multipath signals of wireless networks in complex environments such as outdoor urbanized areas. The propagation model is essentially a 3-D ray tracing process that, in principle, predicts the local mean power received at any given point. For each point, the vector sum of multipath power is computed. The model includes the effects of polarization, material properties, and antenna patterns. Prediction can also account for diffraction effects around corners, which is particularly significant in indoor and outdoor urban propagation environments.

The simulations provide contours of power levels that can be used to predict the maximum received power of the wireless signals. The effects of several systems are examined. Therefore, this research attempts to address the questions: what is the maximum coverage area of UAVs, how many UAVs should be used, what frequency should be used, and what is the signal strength level at the GCS? Systems designers generally address these from the coverage point of view and therefore these questions can be answered by determining the signal contours in the urban area versus frequency.

In order to meet the goals of the thesis, fundamental steps were used to create the propagation simulation:

1. Familiarization with the **Urbana** Toolset and validation of some simple test geometries.

2. Generation of multilevel building models and calculation of wireless signal levels for various UAV system parameters.

3. Simulation of link performance (signal strength level versus system parameters) and analysis of the results to determine what steps can be taken to improve the UAV-GCS command link.

E. THESIS OUTLINE

Chapter II discusses issues of radiowave propagation in urbanized areas. The propagation models are also described. The architecture and hardware used with UAV-GCS networks are introduced. The discussion covers methods of handling the propagation problem, specifically, the **Urbana** Wireless Toolset. A flowchart is presented to illustrate the steps involved in running the **Urbana** program.

Chapter III simulates UAV-GCS data link transmission in urbanized areas. The multipurpose security and surveillance mission platform (MSSMP) UAV was chosen as the test simulation model. The parameters used were obtained from the public domain and, when not possible due to security classification, were generated through logical deduction. UAV was positioned at its typical operating altitude and frequency in various simulations to investigate signal contour patterns.

Chapter IV discusses insights drawn from the simulations, suggestions for future research and applications to the military operations, and presents some conclusions.

II. ISSUES OF URBAN PROPAGATION AND PROPAGATION MODELS

This chapter discusses the main issues of radiowave propagation in urbanized areas and some of the common models (theoretical and empirical) used for predicting signal strength. The operational issues with UAV communication and the **Urbana** wireless toolset are also discussed.

A. RADIOWAVE PROPAGATION IN URBANIZED AREAS

The mechanisms, which govern radio propagation in outdoor urbanized areas, are complicated, but they can generally be attributed to three basic propagation methods: (1) reflection, (2) diffraction, and (3) scattering [2]. As a result of these three propagation mechanisms, the received signal strength at the GCS can be roughly characterized by three nearly independent phenomena of large-scale path loss, large scale shadowing, and multipath fading. UAV-GCS command links in urban environments are subjected to severe degradation due to the combination of these three propagation effects.

1. Reflection

If we assume that a surface can be approximated by an infinite plane separating two media that have different conductivity and permittivity parameters, then equations relating a reflected electromagnetic (EM) wave to its incident EM wave and the dielectric properties of the two media can be obtained. Initially we will assume that the media are infinitely wide so that the surface is the only discontinuity in the environment. Both media, as depicted in Figure 2, are also assumed to be homogeneous, and the surface between them perfectly smooth.

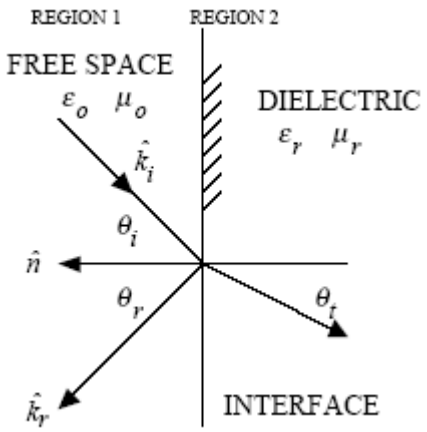

Figure 2. Incident wave on an interface between free space and a dielectric (From Ref. [7].).

For perpendicular polarization (the electric field vector is perpendicular to the plane defined by $\hat{n}$ and $\hat{k}_i$)

$$\Gamma_{\perp} = \frac{\eta \cos\theta_i - \eta_0 \cos\theta_t}{\eta \cos\theta_i + \eta_0 \cos\theta_t} \tag{1}$$

$$E_{r\perp} = \Gamma_{\perp} E_{i\perp} \tag{2}$$

and for parallel polarization (the electric field vector is parallel to the plane defined by $\hat{n}$ and $\hat{k}_i$)

$$\Gamma_{\parallel} = \frac{\eta \cos\theta_t - \eta_0 \cos\theta_i}{\eta \cos\theta_t + \eta_0 \cos\theta_i} \tag{3}$$

$$E_{r\parallel} = \Gamma_{\parallel} E_{i\parallel} \tag{4}$$

where $\Gamma_{\perp}$ = Fresnel reflection coefficient for perpendicular polarization,

$\Gamma_{\parallel}$ = Fresnel reflection coefficient for parallel polarization,

E_i = incident field,

E_r = reflected field, and

η = $\sqrt{\mu/\varepsilon}$.

The planar interface assumption is not a severe limitation in practice. Most building walls are flat compared to the wavelength of interest, and the Fresnel formulas are accurate as long as the reflection point is not near a wall edge. By assuming that the regions under consideration are homogeneous and that wavelength is small compared to the size of the scattering object, we can work in the context of GO and assume ray paths are straight lines [8]. This is the fundamental postulate of ray tracing.

2. Scattering

Surfaces in an urban environment are always, to some degree, rough which affects the reflection of electromagnetic waves. For example, roads laid with bitumen to increase friction are not perfectly smooth. Scattering models will alter the magnitude of a reflected signal and alter its phase. However, if the heights of the surface irregularities are less than $\lambda/16\sin\psi$ (where ψ is the grazing angle of incidence), then the scattering effects of the surface can be ignored [9]. When the surface is smooth, the Fresnel coefficients are accurate and attenuation of the signal due to diffuse reflections is kept to a minimum.

Landron, Feuerstein and Rappaport [10] modified the Fresnel reflection coefficients by a scattering loss factor ρ_s to account for the lower energy caused by rough surface scattering. The parameter ρ_s is defined by

$$\rho_s = \exp\left[-8\left(\frac{\pi\sigma_h \cos\theta_i}{\lambda}\right)^2\right] I_0\left[8\left(\frac{\pi\sigma_h \cos\theta_i}{\lambda}\right)^2\right] \tag{5}$$

where σ_h = standard deviation of the surface height about its mean value, and

I_0 = modified Bessel function of order zero.

3. Diffraction

Diffraction is a phenomenon that is caused by discontinuities in a surface where an electromagnetic wave impinges on that surface. The mechanism results in the discontinuity acting as a radiating point or edge for a fraction of the electromagnetic wave. Thus an electromagnetic wave appears to propagate around a corner or edge.

Keller [11] considered the diffraction caused by an infinite edge of a perfectly conducting plane. A wave incident on an edge produces a cone of scattered components as shown in Figure 3.

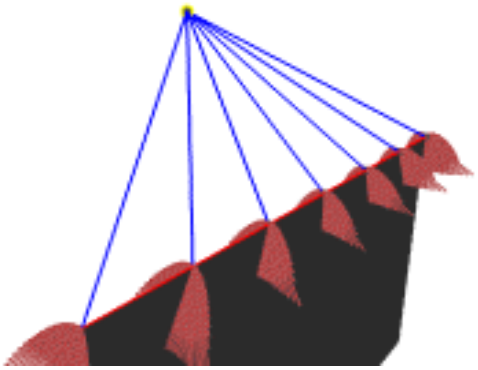

Figure 3. Diffraction at a knife-edge (From Ref. [12].).

For the angles α, β and θ as depicted in Figure 4, the diffraction coefficient is given by

$$D = -\frac{e^{j\frac{\pi}{4}}}{2(2\pi k)^{\frac{1}{2}} \sin\beta}\left[\sec\left(\frac{1}{2}(\theta-\alpha)\right) \pm \csc\left(\frac{1}{2}(\theta+\alpha)\right)\right] \qquad (6)$$

where the first case (positive sign) is used for hard polarization and the second (negative sign) for soft polarization [11].

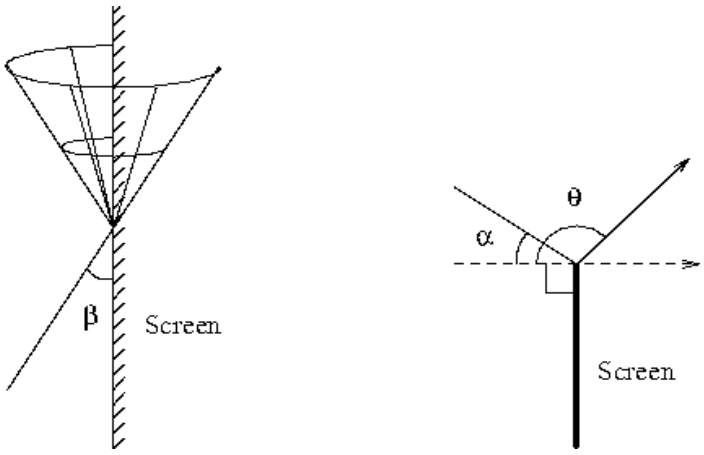

(a) (b)

Figure 4. (a) Elevation view of diffraction. (b) Side view of diffraction (From Ref. [13].).

GTD is an extension to classic geometrical optics/acoustics that allows for treating diffraction phenomena. In the case of radio waves, diffraction cannot be ignored since it can cause radio signals to propagate around obstacles like the corners of buildings in a typical urban area.

Introduced by J. Keller in 1962, GTD models diffraction by considering all wedges (an edge and 2 adjacent surfaces) in the environment as secondary sources of diffracted rays. Any ray impinging on an edge gives rise to a cone of diffracted rays. The amplitude of such diffracted echoes from an edge is defined by a diffraction coefficient that depends on the geometry of the wedge and the incident and outgoing directions of the diffracted ray.

Both GTD and its variant, uniform theory of diffraction (UTD) are widely used techniques for modeling high frequency antennas mounted on various scattering structures [14]. UTD has proven itself to fit nicely in terms of the ray optics format and also provides a means for analyzing the effect of three-dimensional structures such as the wedge [15]. This type of wedge diffraction analysis may be used for modeling propagation effects in the presence of buildings [16].

4. Large-scale Path Loss

The difference between the level of the transmitted signal from the UAV and the signal in the general area of the GCS is generally referred as the path loss, or area mean variation. The area mean power trace is well known to be dependent upon frequency, antenna heights, propagation path length and levels of environment clutter [17]. Path loss can be modeled by

$$PL_{dB}(d) = \overline{PL_{dB}}(d_0) + 10\log_{10}\left(\frac{d}{d_0}\right)^n + X_\sigma \tag{7}$$

where $\overline{PL_{dB}}(d_0)$ = mean path loss at close-in distance d_0 (typically 100 m to 1 km),

d = path distance from transmitter to receiver,

n = path loss exponent, and

X_σ = zero mean Gaussian random variable with standard deviation σ_{dB}.

The value of *n* typically lies between 2 and 5. A value of 2 refers to free space propagation and the variation of the received signal follows the well-known Friss formula [18]. A value greater than 2 indicates the influence of structures on the earth surface, namely infrastructures. Dense urban areas will have a *n* value of at least 4.

5. Lognormal Shadowing

Variability associated with large-scale environment obstacles leads to the local mean power fluctuation about a constant-area mean power over medium distances. This is known as shadowing and is caused by the terrain contour and other obstructions between the UAV and GCS. Egli [19] reported that this variability can be approximated by a lognormal distribution and is independent of the distance.

6. Multipath Fading

The composite signal at the receiver antenna suffers magnitude and phase variations due to the multiple propagation paths that interfere constructively and destructively. The fades occur at approximately half wavelength intervals and at times may drop to 30 dB below the local mean. Ricean fading occurs when there exists a predominant or LOS propagation path between transmitter and receiver. In the case where the average signal occurs from all directions, then the fading is Rayleigh. Typically, Rayleigh fading is dominant in urban radiowave propagation and represents the worst case [20].

B. THEORETICAL MODELS FOR URBAN PROPAGATION

Urban and suburban problems are complicated because the fields in the immediate vicinity of the portable or mobile radio are a superposition of localized mulitpath scattering. This is because the signal strength may vary from peak levels of a few dB above the mean to tens of dB below the peaks in deep fades. Consequently, we may need to rely on statistics to determine the mean and standard deviation of received signals. Two widely distributed models are presented.

1. Diffracting Screens Model

A very simple model of an urban area would consist of a cluster of nearly homogeneous buildings. Walfisch and Bertoni [3, 4] modeled the rows of city buildings as a series of absorbing diffracting screens of uniform height. The forward diffracting, along the screens, with a final diffraction down to the street level gave an overall propagation model for the case of an elevated antenna of an UAV above the building roofline to a GCS at street level.

2. COST 231 Model

This model was created based on the work of Walfisch-Bertoni and Ikegami [21] along with empirical factors. Basically, the model uses Walfisch-Bertoni results to account for the urban environment along with Ikegami's correction functions for dealing with street orientation. The model was applied to the 800-to-1800 MHz bands and successfully tested in the German cities of Mannheim and Darmstadt.

C. EMPIRICAL MODELS FOR URBAN PROPAGATION

Propagation in urban and suburban areas is different from the flat ground plane two-ray model in that a single specular ground reflection rarely exists. Frequently even the direct path is obscured as the receiver is often below building roof level on city streets. This is illustrated in Figure 5. Often, empirical models are city specific and are tied to urban land use maps.

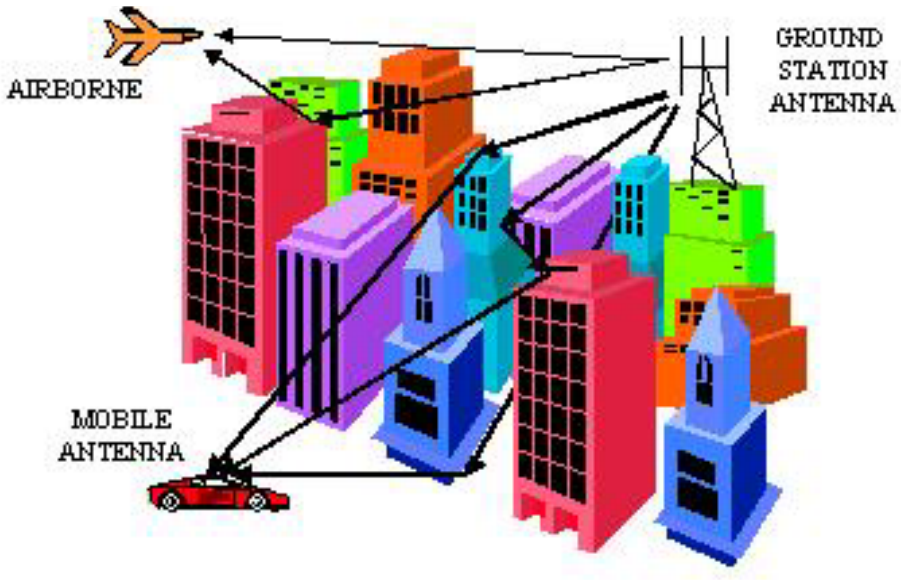

Figure 5. Propagation path of elevated base station to antenna at ground level (From Ref. [7].).

1. Okumura Signal Prediction Model

Okumura's model is one of the most widely used models for signal prediction in urban areas. This model is applicable for frequencies in the range 150 MHz to 1920 MHz (although it is typically extrapolated up to 3000 MHz) and distances of 1 km to 100 km. It can be used for base station antenna heights ranging from 30 m to 1000 m. Okumura developed a set of curves giving the median attenuation relative to free space in an urban area over a quasi-smooth terrain with a base station effective antenna height of 200 m and a mobile antenna height of 3 m. These curves were developed from extensive measurements using vertical polarized omni-directional antennas at both the base and mobile, and are plotted as a function of frequency in the range 100 MHz to 1920 MHz and as a function of distance from the base station in the range 1 km to 100 km. To determine path loss using Okumura's model, the free space path loss between the points of interest is first determined, and then a correction value as read from the curves is added to it, along with correction factors to account for the type of terrain. The model can be expressed as [22]

$$L_{50} = L_F + A_{mu}(f,d) - G(h_{te}) - G(h_{re}) - G_{Area} \tag{8}$$

where L_{50} = 50th percentile value of propagation path loss in dB,

L_F = free space propagation loss $= 4\pi\lambda^2 / R^2$,

λ = wavelength of the propagating wave,

R = distance of free space propagation,

A_{mu} = median attenuation relative to free space,

$G(h_{te})$ = base station antenna height gain factor (base station height, h_{te}),

$G(h_{re})$ = mobile antenna height gain factor (mobile station height, h_{re}), and

G_{Area} = gain due to the type of environment.

Note that the antenna height gains are strictly a function of height and have nothing to do with antenna patterns. Okumura found that both $G(h_{re})$ and $G(h_{te})$ vary at a rate of 20 dB/decade at heights above 3 m but $G(h_{re})$ varies at a rate of 10 dB/decade at heights less than 3 m. G_{Area} is affected by terrain related parameters such as terrain undulation height, isolated ridge height, average slope of the terrain and the mixed land-sea parameter.

2. The Hata and Modified Hata Formulas

The original Hata model was published in 1980. Hata took the information in the field strength curves produced by Okumura and produced a set of equations for path loss. Two of the limitations of the Hata model are that it has a restricted path length and a restricted frequency range. A number of modified models have been produced to extend the path length and frequency range. These modified models vary slightly from each other and some of these models more closely match the Okumura curves than do others.

The Hata empirical model uses a propagation equation split into two terms: a term that has a logarithmic dependence on distance and a term that is independent of distance. The Hata model also includes adjustments to the basic equation to account for urban, suburban, and open area propagation losses. The Hata equation for propagation loss in an urban area is given by [23]

$$L_p = 69.55 + 26.16\log(f) - 13.82\log(h_b) + [44.9 - 6.55\log(h_b)]\log(d) + a_x(h_m) \quad (9)$$

where f = frequency in MHz,

h_b = height of base station, and

$a_x(h_m)$ = height correction function.

In a medium city, the height correction function is in the form

$$a_m(h_m) = [0.7 - 1.1\log(f)]h_m + 1.56\log(f) - 0.8, \quad (10)$$

and in a large city below 200 MHz

$$a_2(h_m) = 1.1 - 8.29\log^2(1.54h_m). \quad (11)$$

Modified Hata models were subsequently produced to improve on the range limitation of the original Hata model.

D. OPERATIONAL ISSUES WITH UAV COMMUNICATION

Airborne data link rates and processor speeds are in a race with respect to enabling future UAV capabilities. Today, and for the near term, the paradigm is to relay virtually all-airborne data to the ground and then process it there for interpretation and decisions. Eventually, however, onboard processing power will outstrip data link capabilities and allow UAVs to relay the results of their data, vice the data itself, to the ground for decision making. At that point, the requirement for data link rates in certain applications, particularly imagery collection, should drop significantly.

Meanwhile, data compression will remain relevant into the future as long as band-limited communications exist, but it is unlikely that compression algorithms alone will solve the near-term throughput requirements of advanced sensors. A technology that intentionally discards information is not the preferred technique. For now, compression is a concession to inadequate bandwidth.

In the case of radio frequency (RF) data links, limited spectrum and the requirement to minimize airborne system size, weight, and power (SWAP) have been strong contributors for limiting data rates. Rates up to 10 Gbps (40 times currently fielded

capabilities) are considered possible at current bandwidths by using more bandwidth-efficient modulation methods. Currently fielded digital data links provide an efficiency varying between 0.92 and 1.5 bps/Hz, where the theoretical maximum is 1.92 [24]. At gigahertz frequencies, however, attenuation due to precipitation becomes pronounced. Attenuation may be caused by absorption, in which the raindrop, acting as a poor dielectric, absorbs power from the radio wave and dissipates the power by heat loss or by raindrop scatter.

Airborne optical data links, or lasercom, will potentially offer data rates two to five orders of magnitude greater than those of the best future RF systems. Although lasercom could surpass RF in terms of airborne data transfer rate, RF will continue to dominate at the lower altitudes for some time into the future because of its better all-weather capability.

1. Relay Coverage

A study [25] conducted by United States Office of the Secretary of Defence/C3I regarding the use of a UAV as an Airborne Communication Node (ACN) concluded:

- Tactical communication needs can be met much more responsively and effectively with ACNs than with satellites.
- ACNs can effectively augment theater satellite capabilities by addressing deficiencies in capacity and connectivity.
- Satellites are better suited than UAVs for meeting high capacity, worldwide communications needs.

ACNs can enhance intra-theater and tactical communications capacity and connectivity by providing more efficient use of bandwidth, extending the range of existing terrestrial LOS communications systems, extending communication to areas denied or masked to satellite service and providing significant improvement in received power density compared to that of satellites, improving reception and decreasing vulnerability to jamming. ACNs can also provide valuable communications for troops in military operations in urban terrain (MOUT) as depicted in Figure 6.

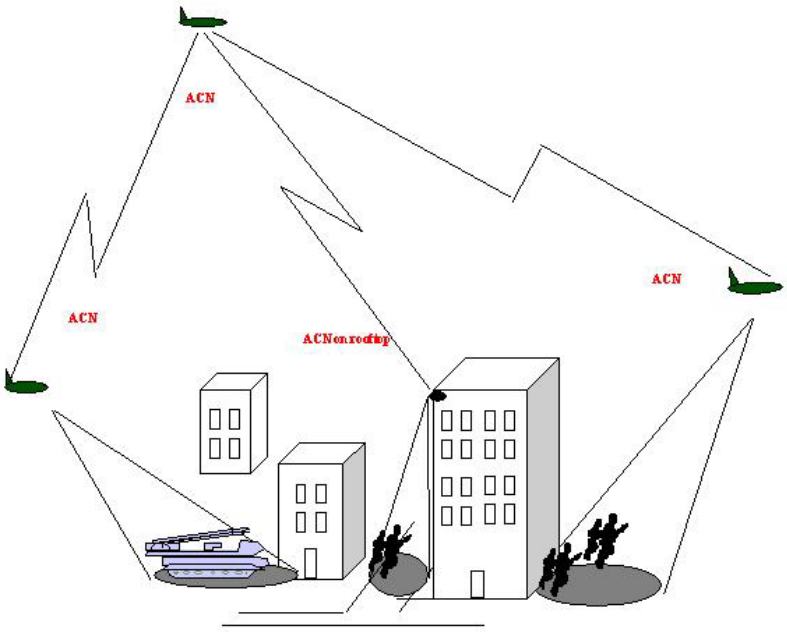

Figure 6. ACN providing communication coverage for troops in urban terrain.

2. Portable Ground Control Station (PGCS)

Agents sitting in a static building, which afforded large and heavy equipment, probably orchestrated the Yemen Predator strike. However, during MOUT, assaulting troops will most likely have only the luxury of a small portable system. The vehicle operator will control the UAV via the telemetry (TM) data stream using the portable ground control station (PGCS). The PGCS can be interfaced to numerous types of simplex, half, or full duplex RF systems for flexible communications requirements. A simplex RF system provides increased flight and payload control capabilities over a model aircraft remote control system. A half or full duplex RF system increases flexibility by providing TM downlink capabilities allowing the addition of sensors such as a global positioning system (GPS) for position information. With the bi-directional communication links and GPS, the vehicle provides its position in latitude, longitude format within the TM data. This allows the PGCS to track and command the UAV. A typical PGCS might consist of three basic modules, namely the display module, portable controller and transceiver.

E. URBANA WIRELESS TOOLSET

Indoor and outdoor wireless networks are increasingly popular and there has been a significant interest in design tools. While there are several engineering tools to predict antenna radiation and wave propagation, Science Applications International Corporation's (SAIC) **Urbana** has been selected for this research. The **Urbana** wireless toolset offers a solution for predicting multipath signals of wireless networks in complex environments such as the exterior of an urbanized area. The propagation model is essentially a three-dimensional ray-tracing process that in principle predicts the local mean power received at any given point. For each point, the vector sum of multipath power is computed. The model includes the effects of polarization, material properties, and antenna patterns. Prediction can also account for diffraction effects around corners, which is particularly significant in indoor and outdoor urban propagation environments. It is a UNIX-based toolset comprised of the following components:

1.) **XPatch**

2.) **XCell**

3.) **Cifer** and

4.) **Urbana**.

Given building data, systems parameters, and antenna locations, **Urbana** determines received power levels at specific points throughout a spatial area. There are several electromagnetic algorithms to select from, but all are based on a high frequency assumption. The size of the scattering objects is assumed to be much larger than a wavelength, which is satisfied by the known operating frequencies of the UAVs used for this research.

The **XPatch** or **XCell** GUI displays a three-dimensional model and perspective views of signal strengths in and around the building. Transmitting parameters were selected to represent a possible UAV-GCS network system. The relationship between the suite of programs is illustrated in Figure 7. The components of the toolset are discussed in the following sections.

STEP 1: GENERATING INPUT DATA FILES

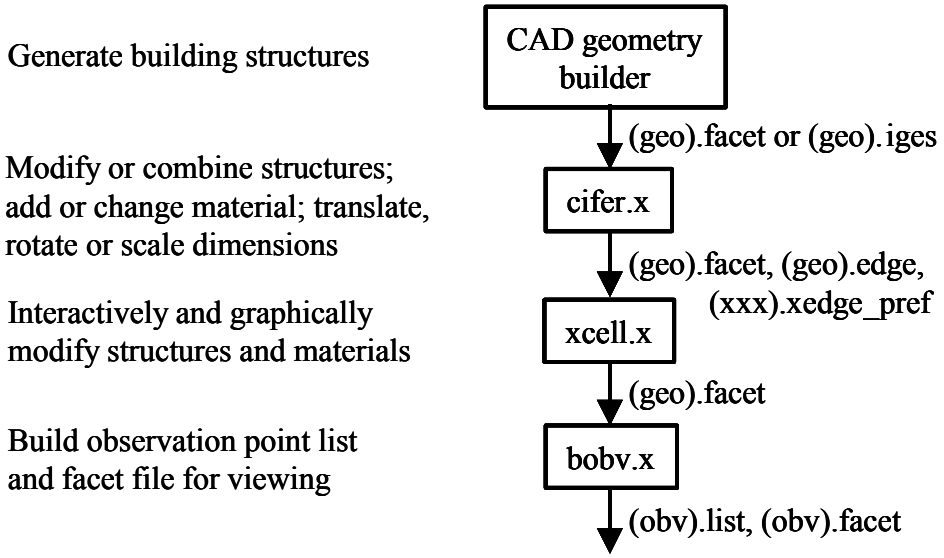

STEP 2: GENERATE URBANA INPUT FILE AND RUN URBANA

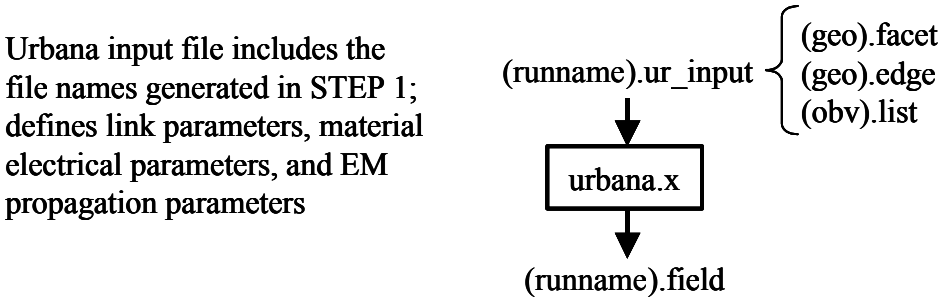

STEP 3: POST PROCESSING

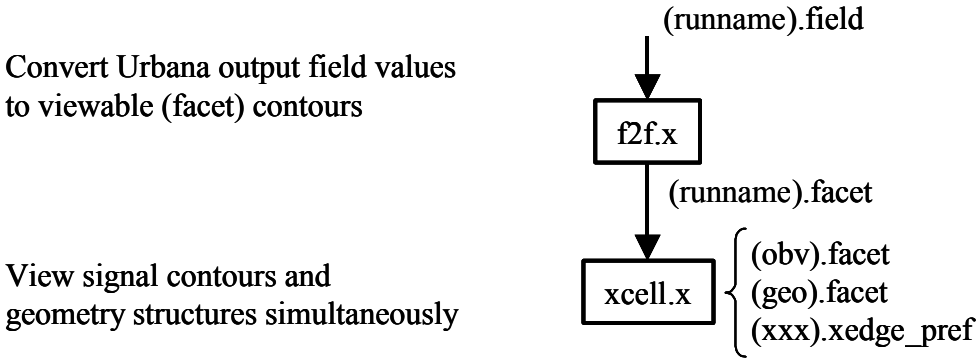

Figure 7. Urbana flowchart.

1. Silicon Graphics Workstation

Two computers were used with the **Urbana** Toolset. The first (EMAG 2) is a UNIX-based Silicon Graphics Indigo Workstation computer with the following ratings: a 150-MHz IP22 processor, data cache size of 16 kB, and main memory size of 320 MB. The second (EMAG 4) is a slightly newer SGI Octane workstation with the following ratings: a 300-MHz IP32 processor, data cache size of 32 kB, and main memory size of 1 Gb.

2. Xcell, Xpatch, and Cifer

Xcell and **Xpatch** are similar graphic user interface programs that are used to visualize the facet models and the results of the propagation simulations of **Urbana**. **Xpatch** was originally designed for scattering and radar cross-section analysis, such as producing and analyzing scattering data for realistic aircrafts, missiles, ships, spacecrafts, and ground vehicles. **Xcell** is an outgrowth of **Xpatch** tailored for wireless propagation modeling.

3. Urbana

Urbana is the primary computational electromagnetic tool for simulating wireless propagation and near-field scattering in complex environments. The underlying ray-tracing physics engine aggregates physical optics, geometric optics, and diffraction physics to produce a high-fidelity three-dimensional simulation.

Through the three-dimensional visualization interface, the user can study and assess antenna and system designs in a wide range of realistic scenes, such as urban environments, building interior and automobile traffic.

Urbana provides wireless system planners with a powerful tool to simulate propagation in outdoor urban settings. The **Urbana** ray-tracing engine can account for the complex, multi-bounce effects introduced by multiple walls and other partially penetrable boundaries in an outdoor environment.

The key inputs to the **Urbana** code are:

- CAD facet models for terrain and buildings.

- Observation regions that conform to the terrain and buildings.
- Surface material properties (e.g., concrete, earth, glass, dielectrics).
- Placement, strength, and vector polarized antenna patterns of transmitters and receivers.

The key outputs are:

- Composite field level at each observation or coverage region sampling point.

Urbana's modeling tools allow engineers to analyze affected EM observation points that arise from the physical complexity of the environment with an emitter. Its three-dimensional capability reveals regions of relatively strong or weak signal levels and provides a diagnostic tool for interpreting the results.

In the next chapter, **Urbana** is used to simulate the performance of several UAV data links in various urban terrains.

III. URBANA SIMULATION

This chapter discusses the platform and system parameters used for simulation. Scenarios depicting realistic deployment of UAVs and GCS locations are modeled and the simulation results are discussed.

A. MULTIPURPOSE SECURITY AND SURVEILLANCE MISSION PLATFORM

The multipurpose security and surveillance mission platform (MSSMP) shown in Figure 8 is designed to provide a rapidly deployable, extended-range surveillance capability for a variety of operations and missions, including: fire control, force protection, tactical security, support to counter drug and border patrol operations, signal/communications relays, detection and assessment of barriers (i.e., mine fields, tank traps), remote assessment of suspected contaminated areas (i.e., chemical, biological, and nuclear), and even resupply of small quantities of critical items.

Figure 8. MSSMP UAV (From Ref. [26].).

The GCS, shown in Figure 9, is highly portable and can be deployed in both open areas and inside buildings.

Figure 9. Portable GCS of MSSMP (From Ref. [26].).

B. SIMULATION PARAMETERS

A vertically polarized dipole antenna transmitting at 5 GHz at power of 1 W was used to simulate a data signal from the MSSMP. The value of 1 W was chosen as a conservative but technologically possible power level for the category of small UAVs. Commercial wireless networks are known to transmit at 100 mW. Meanwhile the Predator UAV, with a payload of over 1000 kg, transmits at 50 W. The thickness of the surface along with the dielectric constant values $\varepsilon = \varepsilon' - j\varepsilon''$, conductivity σ and resistivity R_s of the material was set to simulate walls made of concrete. Roads were simulated with a thin layer of concrete over a semi-infinite plane. A combination of GO and GTD techniques were used in computation of the signal contours.

1. Building Models Used for Simulation

a. Major Suburban Intersection

Using the flowchart steps provided in Chapter II, realistic building propagation models were developed. The first model, as depicted in Figure 10 and Figure 11, represents a mixed cluster of buildings at a major suburban intersection. The size of the observation plane is 560 m × 800 m. The average height of buildings is 40 m. Roads are modeled as concrete lines while buildings are modeled as concrete blocks.

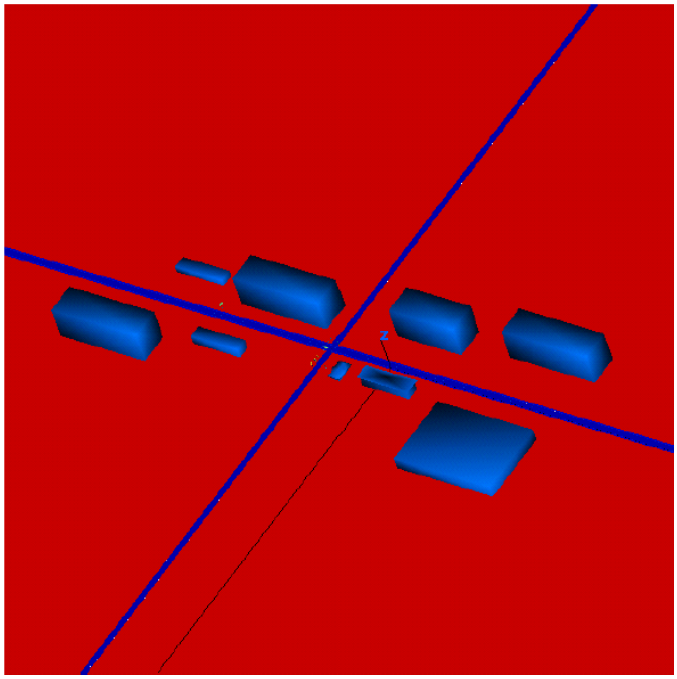

Figure 10. Three-dimensional view of major suburban intersection.

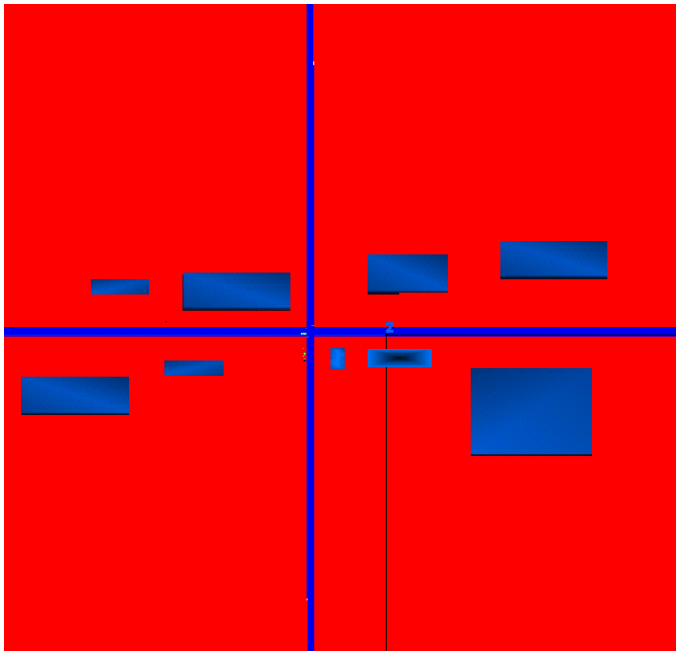

Figure 11. Two-dimensional view of major suburban intersection.

b. Central City Area

A second more complicated and denser model, shown in Figure 12 and Figure 13, represents a central city area with a random distribution of high-rise and low buildings. The size of the observation plane is 1620 m × 800 m. The average height of buildings is 80 m with the tallest at 357 m. Roads are modeled as concrete lines while buildings are modeled as concrete blocks.

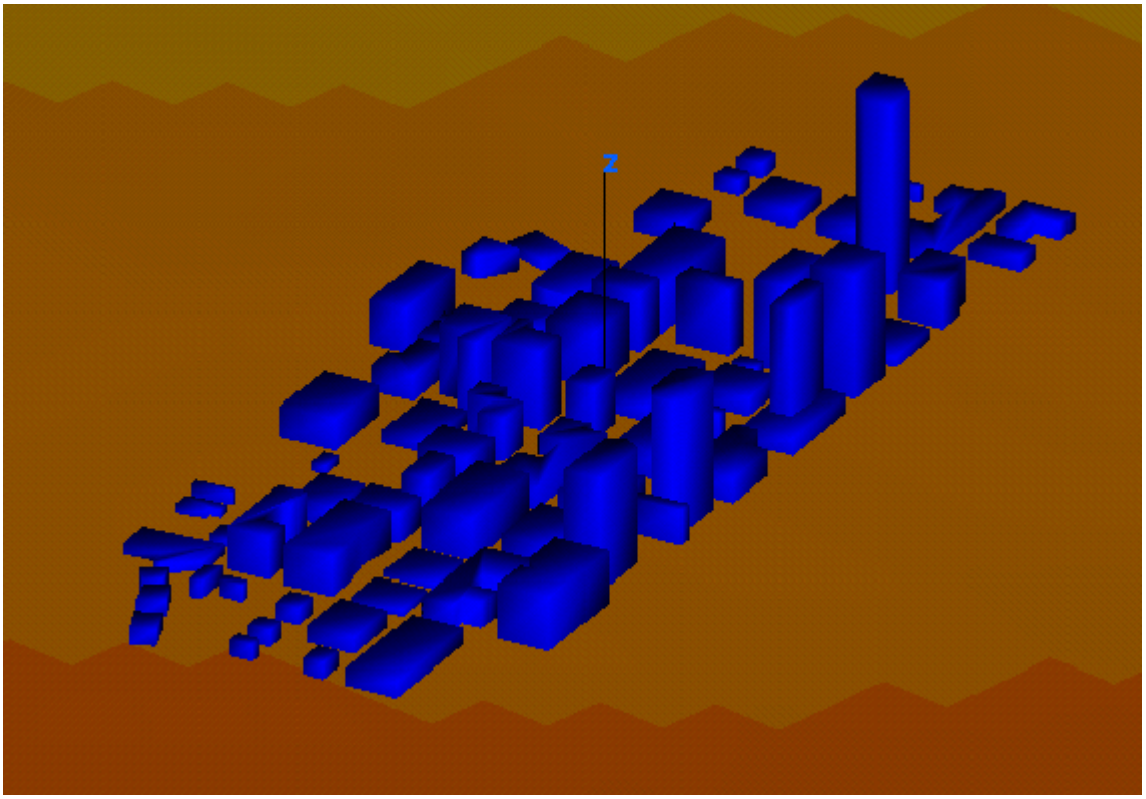

Figure 12. Three-dimensional view of central city area.

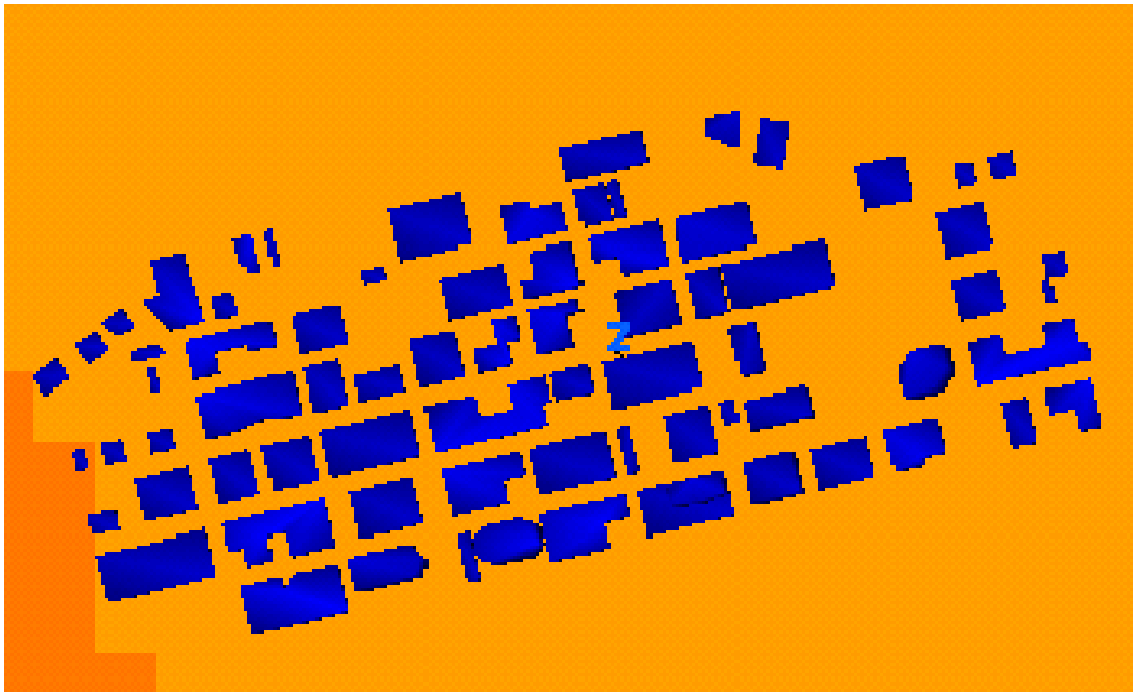

Figure 13. Two-dimensional plan view of central city area.

c. One-level Building

Figures 14 through 17 represent a variation of a one-level building. The size of the base building is 800 in × 800 in with a height of 132 in.

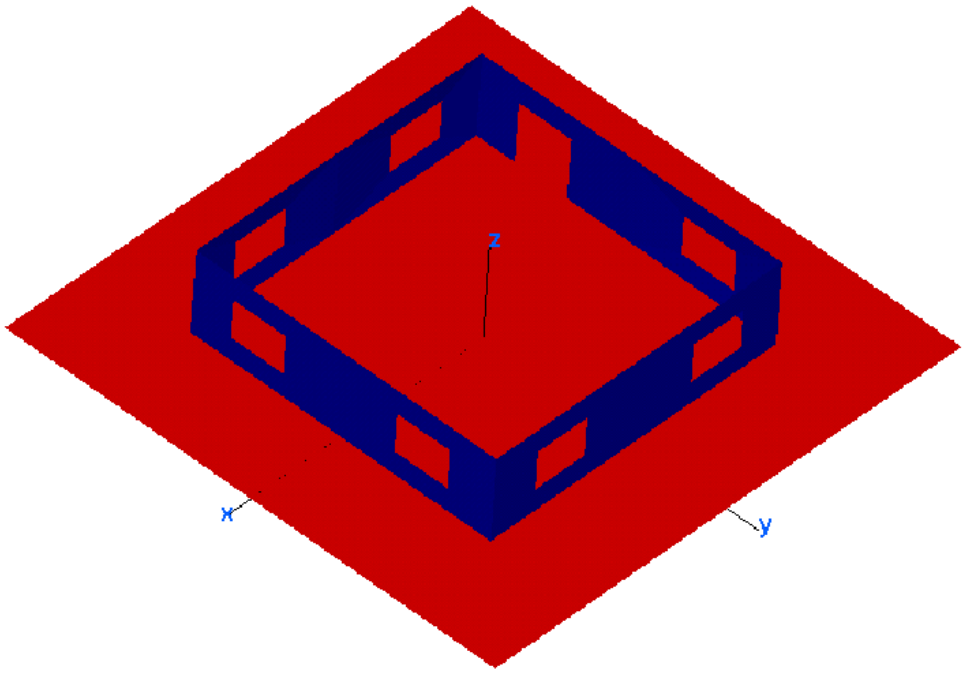

Figure 14. One-level building.

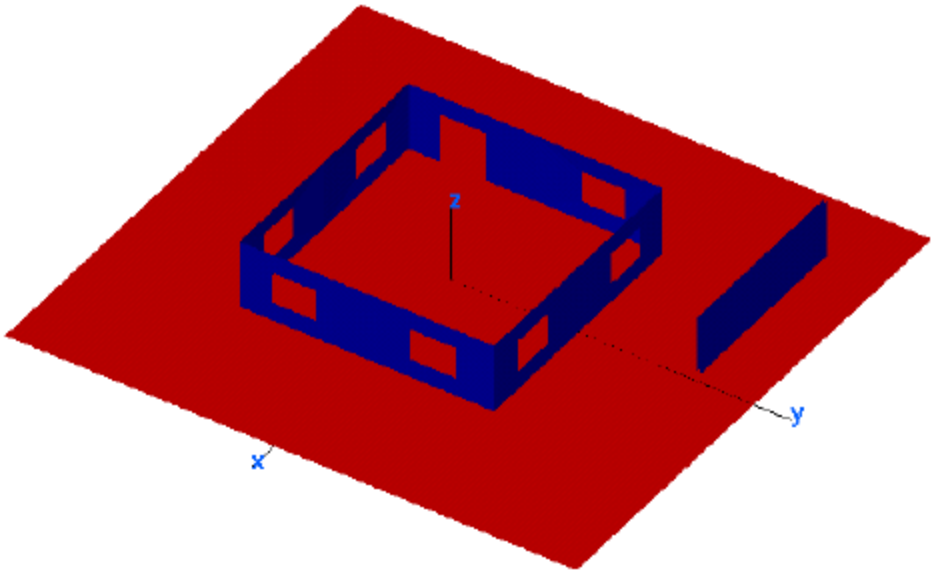

Figure 15. One-level building with barrier wall.

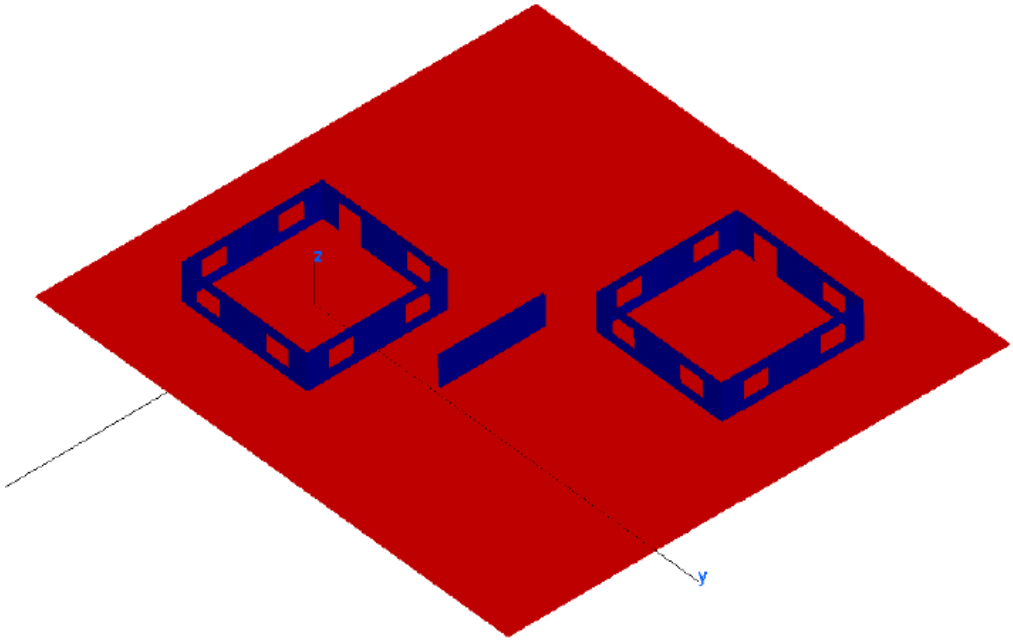

Figure 16. Two buildings with barrier wall.

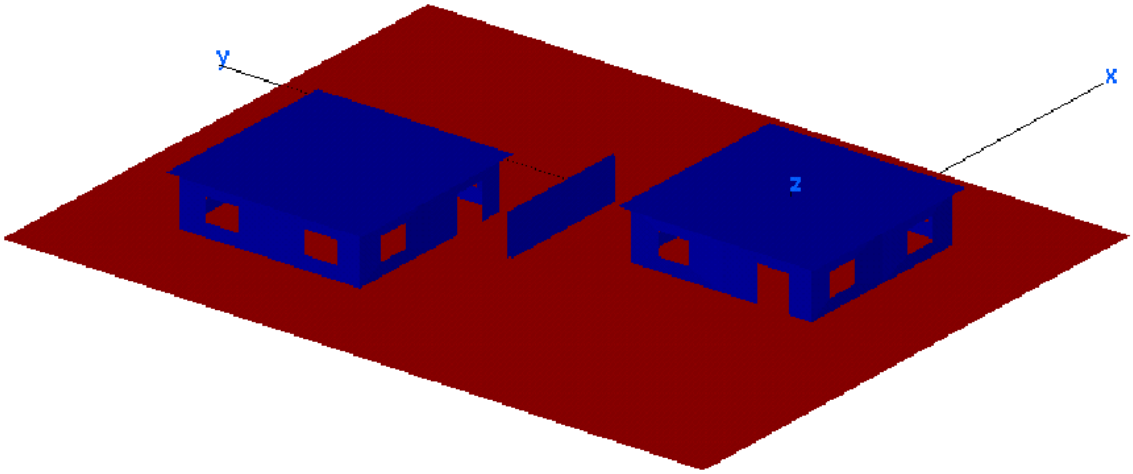

Figure 17. Two houses with barrier wall.

2. Generating Observation Points

The observation area of interest has the same dimensions as the ground plane. The original file of the ground plane can also be used as the name of the facet file describing the terrain. The script file (read by the program ***bobv.x***) for generating the observation points (Filename: *filename.obv*) consists of the following lines:

filename.facet

0.0254

1 1 10

1

– 1000.0 1000.0 – 1000.0 1000.0 1.0 0.0

The first line indicates the name of the file describing the terrain and the second line (input value of 0.0254) converts the unit of length to inches. The third line states the number of observation blocks. The fourth line describes the block type where 1 represents rectangular region and 2 represents a line. The fifth line describes the observation area which in this case is a rectangular region centered on the origin of the XY plane, the size of the footprint (1.0) and the delta offset along the *z*-axis (0.0).

Once all the inputs are specified, the observation program was executed (***bobv.x***) and an observation list file (*filenameg.list*) and observation facet file were created. **XCell** is used to view the observation points as depicted in Figure 18.

Observation Area

Unit Length: Meters
X (-1000, 1000)
Y (-1000, 1000)
Z (0, 0)
Footprint size: 1 inch

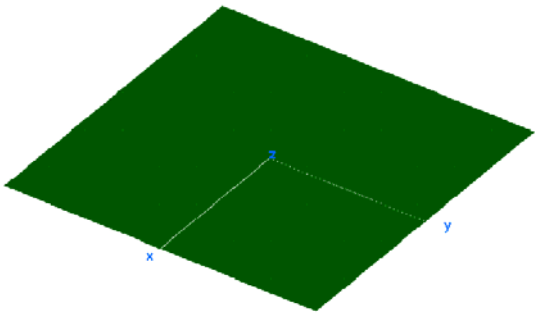

Figure 18. Building observation points as viewed in **Xcell**.

3. Displaying Results

The **Urbana** input file (*vertical_plane.ur_input*) is first created. The input file is ASCII text with a specific set of input code words. The code word arguments are calculation parameters that are modified as needed. Table 1 lists some of the parameters specified in the input file. **Urbana** simulations were subsequently run using the input file (*filename.ur_input*) by executing *urbana filename 0*.

Input Parameter	Values/Option
Facet Model	*filename.facet*
Length Unit	meter
Frequency	5.0 GHz
Antenna Description	ByFile: *dummy.antenna*
Antenna Type	Dipole
Antenna Origin	0.0, 0.0, 0.0
Observation Points	*filename.list*
Rx Antenna	No
Computation Method	GO (geometric optics)
Edge Diffraction	Yes (UTD)
Edge Model	*filename.edge*
Ray Spacing	2.0 degree
Max Bounces	10
Materials	ICOAT = 1
ADVANCED FEATURES	Off

Table 1. Urbana input parameters.

An output file (*filename.field*) will be generated that contains the computed signal levels. Executing the program ***f2f.x*** translates the field results into a color-coded facet file (*filenamefield.facet)* that can be loaded into **XCell** for visualizing the RF signal contours. The displayed data consists of an outline of the model's edge and the color-coded power contour. The input sequence for ***f2f.x*** is shown in Table 2.

Requested Input	Response
Type of E-Field	Magnitude of E-Tot
Number of Field Files	1
Name of Field File	*filename.field*
Antenna Power Level	10 dBm
Histogram Interval	5 dB
Max and Min Clip values	−80 dBm, 10 dBm
Max and Min Range values	−50 dBm, 10 dBm
Number of Levels	25
Lowest Coating Code	1
Name of Output Facet File	*filenamefield*
Side of Footprint Square	1
Shift according to Z-data	Y
Enter z-offset footprint	0

Table 2. Inputs for ***f2f.x***.

C. SCENARIOS AND SIMULATION RESULTS

1. Three-dimensional Ray Tracing Method

In **Xcell**, antennas can be placed anywhere to simulate a transmitter onboard a UAV. Antennas can be set to transmit at different ray angles. The number of diffracted rays can be limited. During visualization, rays from a specific range of diffraction bounces can be chosen. In Figure 19, the dipole antenna transmitting at 1 W is placed at the roof of the tallest building at (-385 m, -7 m, 358 m) and only the 9^{th} to 10^{th} bounces are shown. Three-dimensional ray tracing can be used deterministically for initial signal coverage confirmation at various locations, but it does not, however, calculate the signal strength level at each observation point.

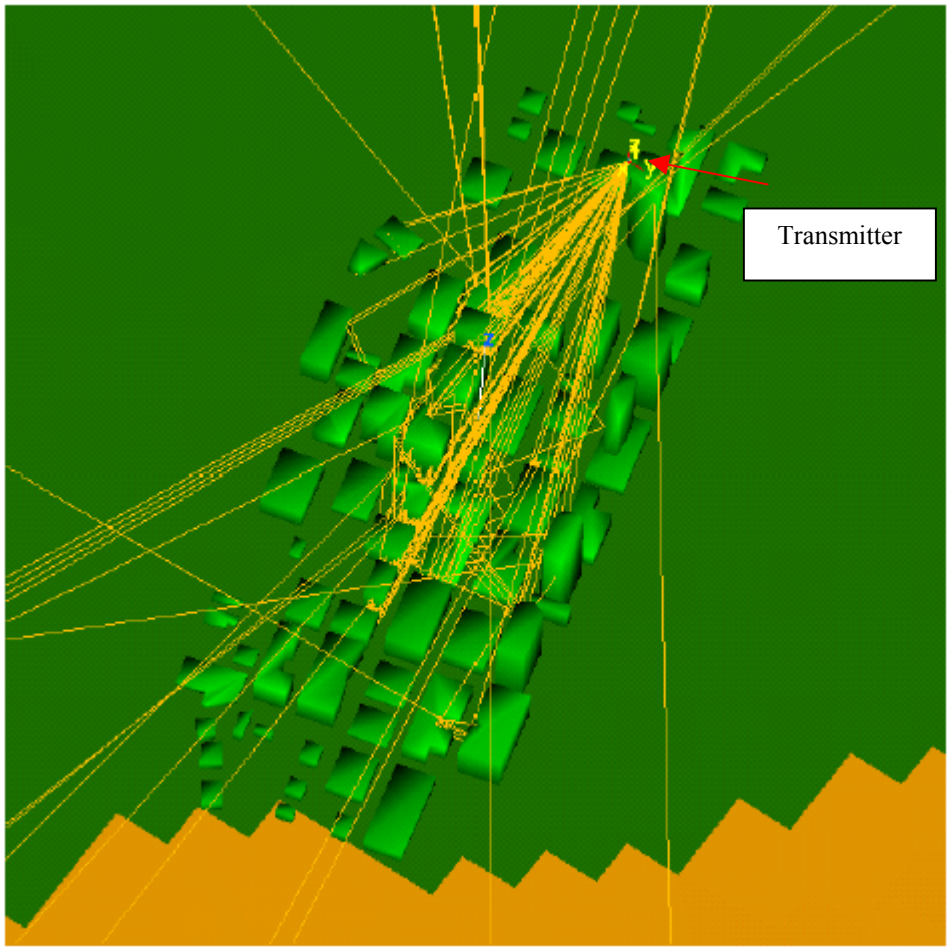

Figure 19. Three-dimensional ray tracing.

Figure 20 depicts a scenario where the signal can only be received by antenna 1 and antenna 2, but not antenna 3. The propagation paths of signals from antennas 1 and 2 are shown. Antenna 3 is in the shadow region with respect to the transmitter.

Figure 20. Signal coverage by deterministic ray tracing.

2. Urban Canyon

The main feature of an urbanized area is the presence of long straight avenues of roads and pavements with buildings on both sides, thus forming a canyon. Similar to surface wave ducting, the effect of urban canyons is clearly visible (green line) in Figure 21 as a corridor for radiowave propagation.

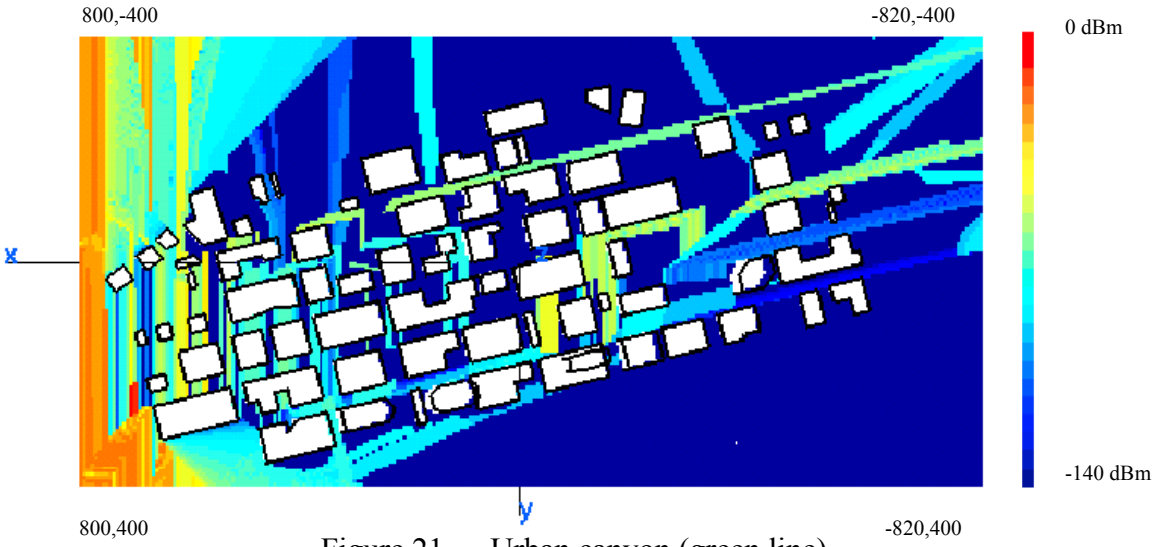

Figure 21. Urban canyon (green line).

In this scenario, the UAV is positioned at (752 m, 203 m, 150 m) at the bottom left of the city. The signal strength drops rapidly due to path loss. For most of the city, the signal strength is at −100 dBm or less. However, it is observed that at certain longitudinal axes across the city, radio waves propagate without much attenuation. These data translate to the capability that in certain parts of the city, despite having no LOS, troops are still able to receive and transmit with higher headquarters (HHQ) through ACNs. Tactically, identification of urban canyons becomes crucial to have total communications coverage throughout the military operation with the minimal logistics tail.

3. Flying UAV Across A City

In this scenario, the UAV is flown across the city along the *x*-axis in support of troops advancing from the right. The altitude of the UAV is kept constant at 358 m, which is just above the tallest building in the city. The *y*-coordinate is maintained constant at −7 m. Figures 22 to 28 depict the signal contours in the city as the UAV moves across the city.

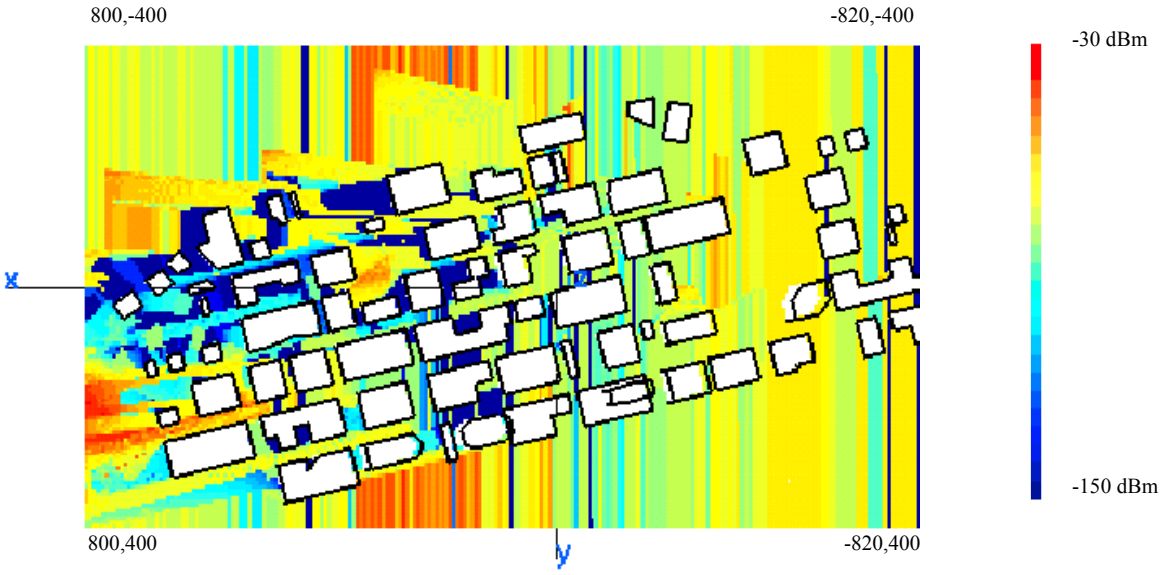

Figure 22. UAV flying across a city, currently at $x = -1200$ m.

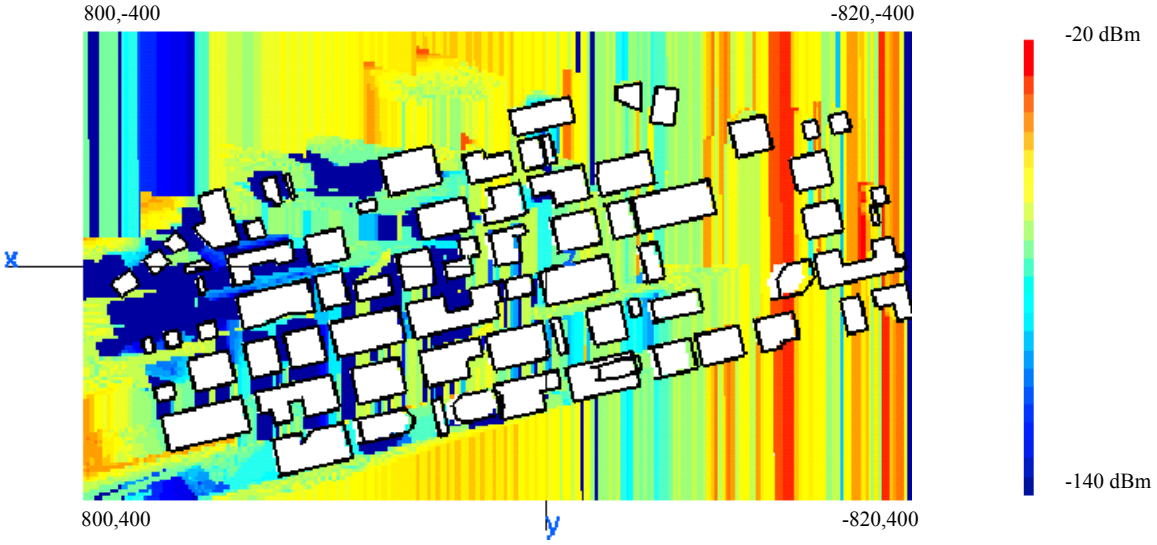

Figure 23. UAV flying across a city, currently at $x = -800$ m.

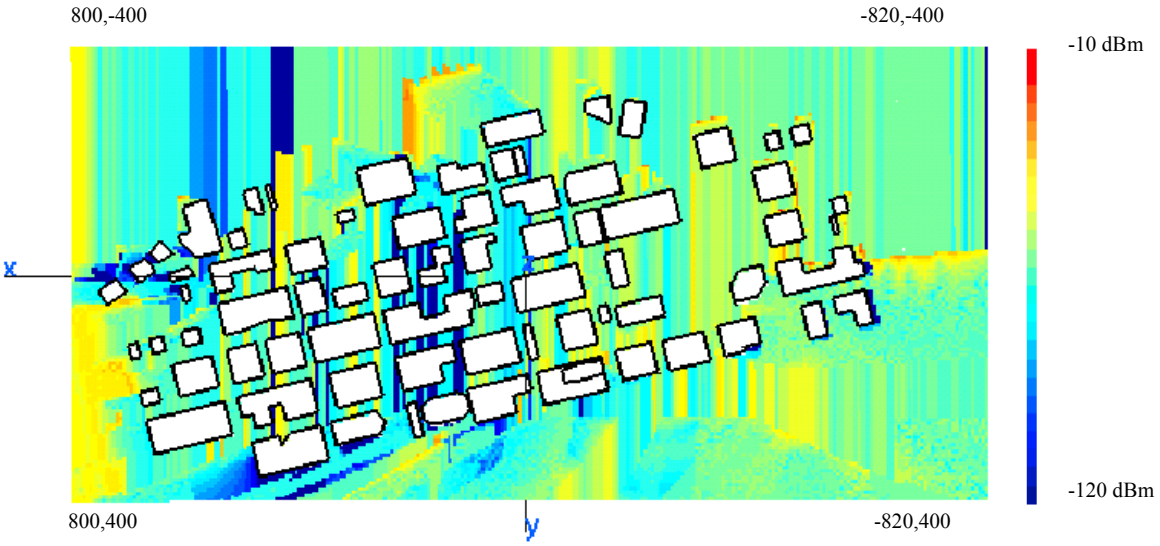

Figure 24. UAV flying across a city, currently at $x = -385$ m.

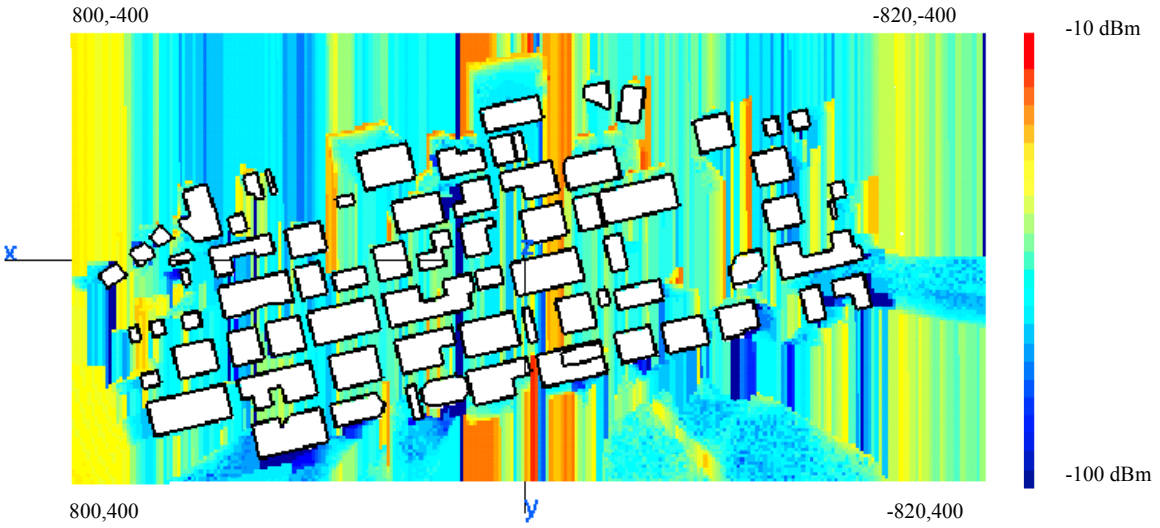

Figure 25. UAV flying across a city, currently at $x = 0$ m.

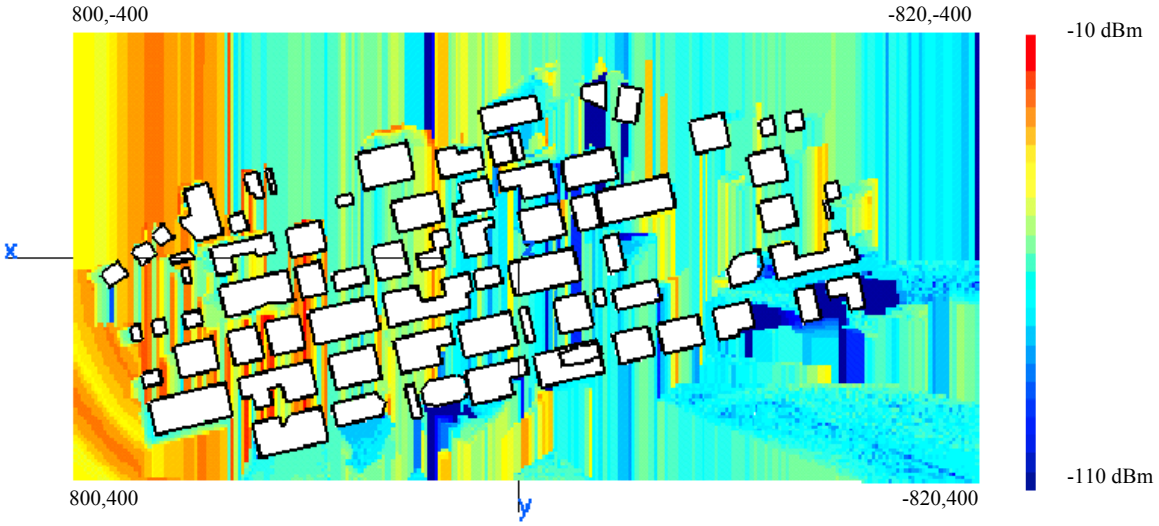

Figure 26. UAV flying across a city, currently at $x = 400$ m.

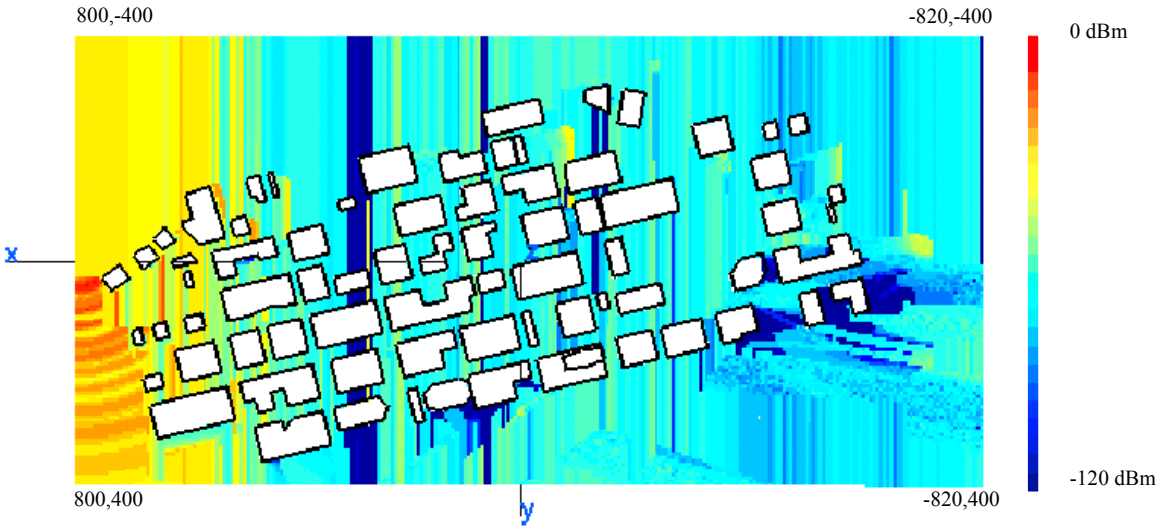

Figure 27. UAV flying across a city, currently at $x = 800$ m.

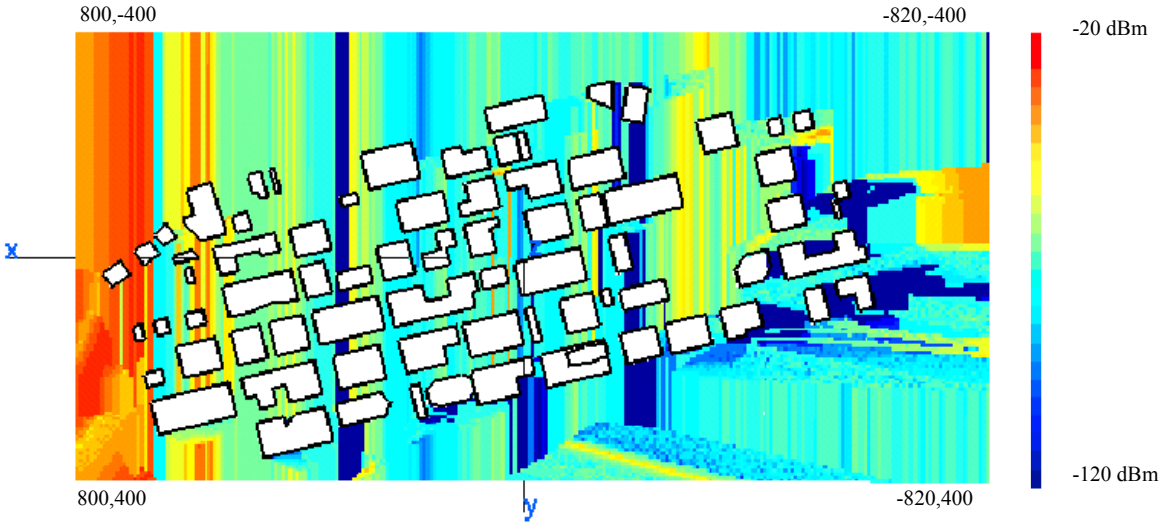

Figure 28. UAV flying across a city, currently at $x = 1200$ m.

The series of figures clearly shows signal contours will change significantly in actual flight operations of a UAV. It is also important to highlight the shifting of shadow regions. In order to achieve the required signal strength level for an effective UAV-GCS link, it is necessary to pre-study the changes of signal contours and to locate, if possible, the ideal location for GCS. The above figures suggest that, given the relatively weak transmission power of both UAV and GCS, the location of the GCS will need to displace with the advance of the UAV, and that the final position be near the left edge of the city. This scenario highlights the needs of a UAV deployed in support of MOUT to have the inherent capability to hover to capitalize on communications opportunities.

4. Deploying Two UAVs

In this scenario, two UAVs were deployed at various locations to investigate the effects on signal contours in the city. Both UAVs transmitted with the same power, and frequency, and the transmissions are coherent in phase. In Figure 29, UAVs were deployed left and right outside of the city boundary at (752 m, 203 m, 150 m) and (-634 m, 140 m, 150 m). Comparing with Figure 21, it is observed that, with an additional UAV, there was an improvement in signal level for most parts of the city. However, the center of city was still shadowed.

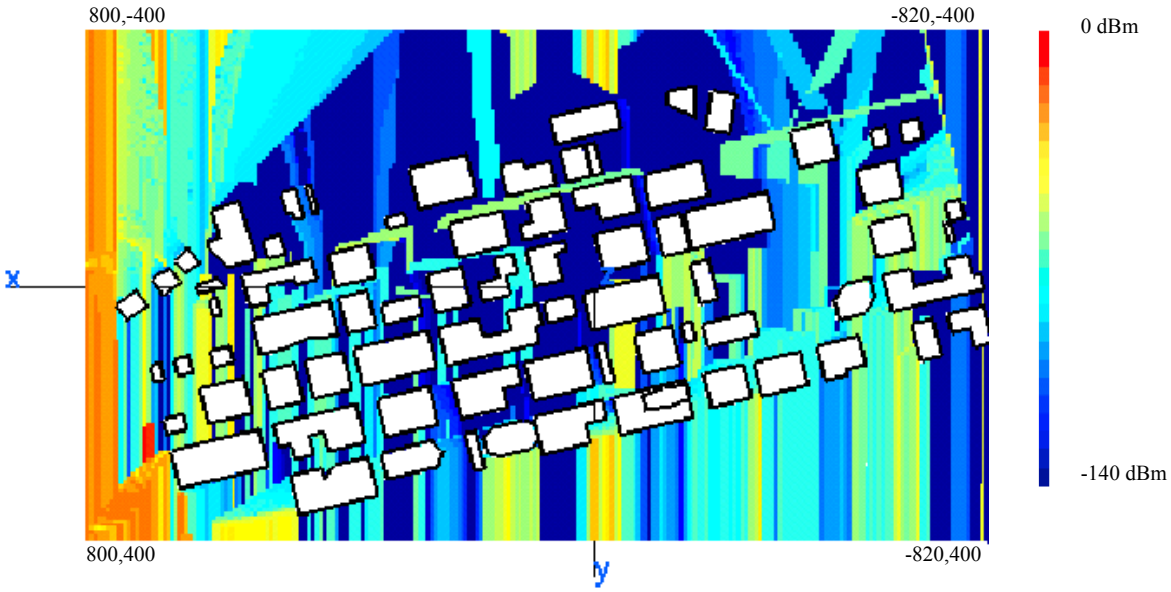

Figure 29. Two UAVs outside city boundary.

Next, the UAV deployed at the right was modeled to hover near the tallest building in the city at (−400 m, −7 m, 358 m) while the other UAV is at the left of the city (400 m, −7 m, 358 m). Figure 30 depicts the signal contour pattern.

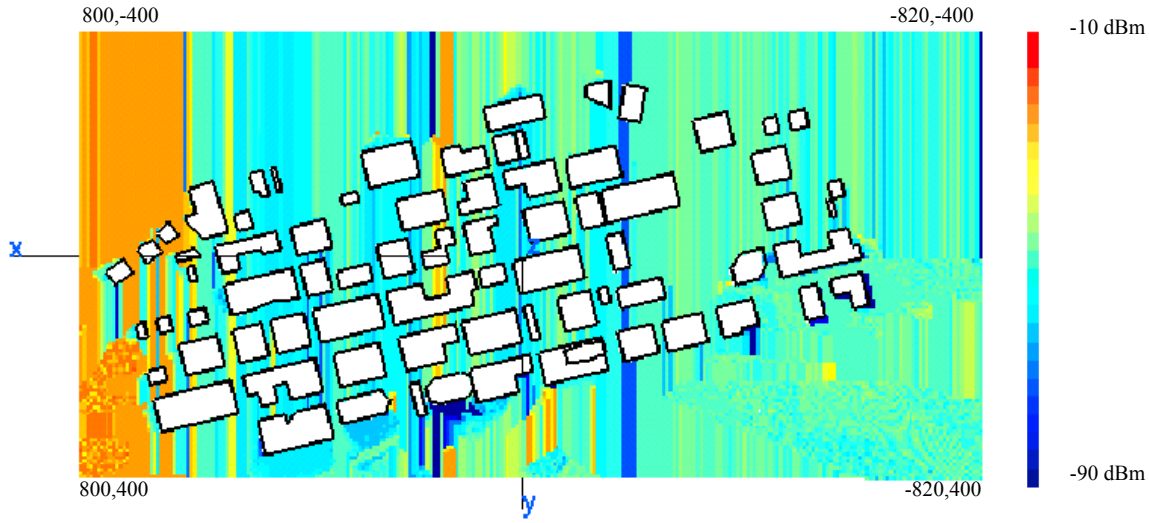

Figure 30. Two UAVs inside city boundary.

A large part of the city has signal strength above −40 dBm. By varying altitude and position, the optimal deployment locations for two UAVs was investigated. Coordinates (410 m, 20 m, 200 m) and (−385 m, −7 m, 358 m), which were near the

tallest buildings in their regions, were used for the final simulation and the signal contour is shown below in Figure 31. The overall contour within the city was moderately good especially in the left region of the city.

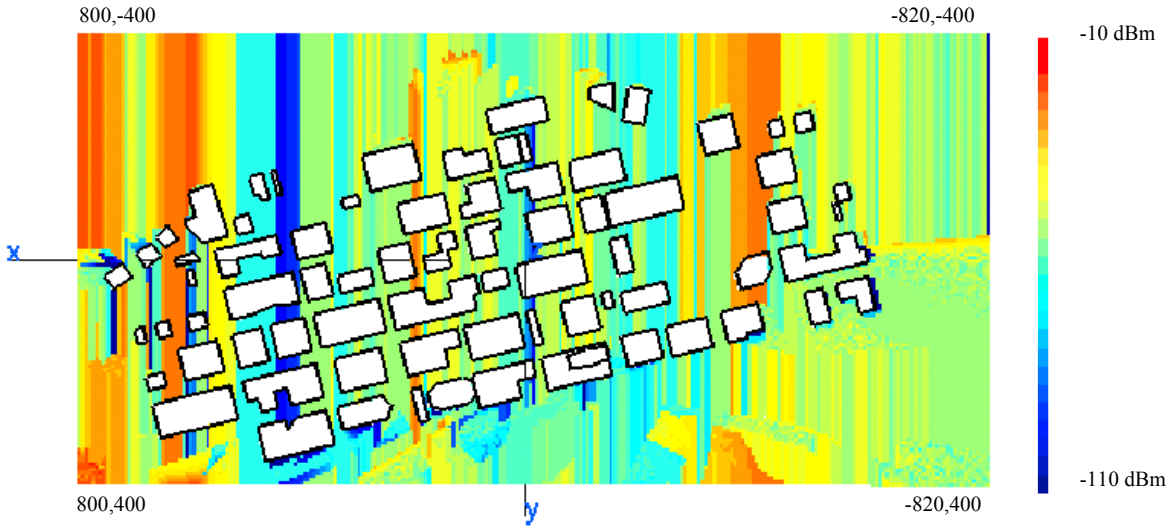

Figure 31. Ideal location for two UAVs inside city boundary.

In the next scenario, the parameters of two UAVs were similar to that used in Figure 30. However, the phase difference of the second UAV transmitter was set at $\pi/2$ and π relative to the first UAV's transmitter. The resulting signal contours are shown in Figures 32 and 33.

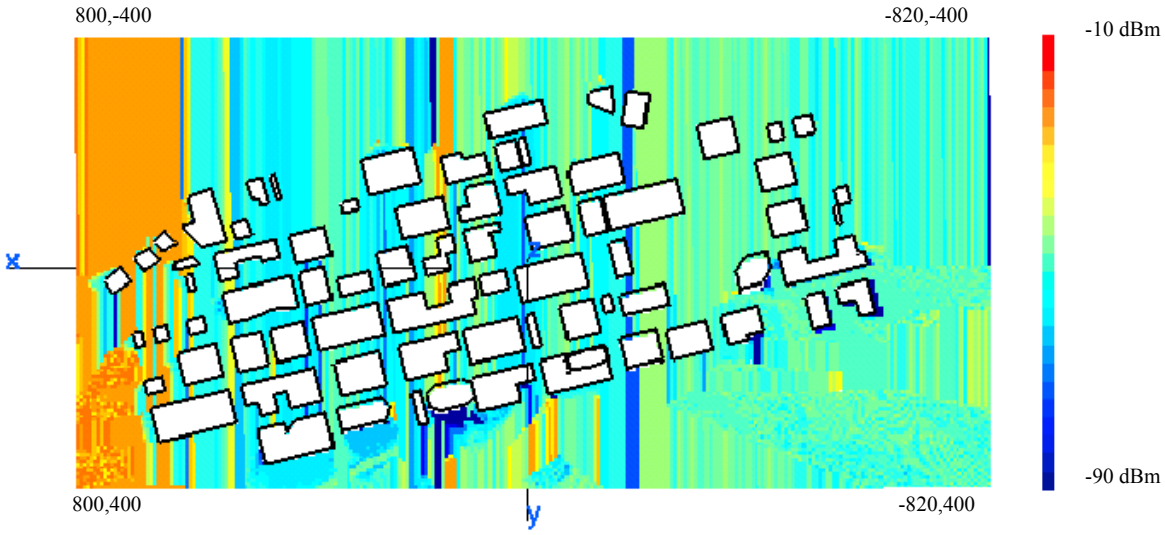

Figure 32. Two UAVs transmitting with a phase difference of $\pi/2$.

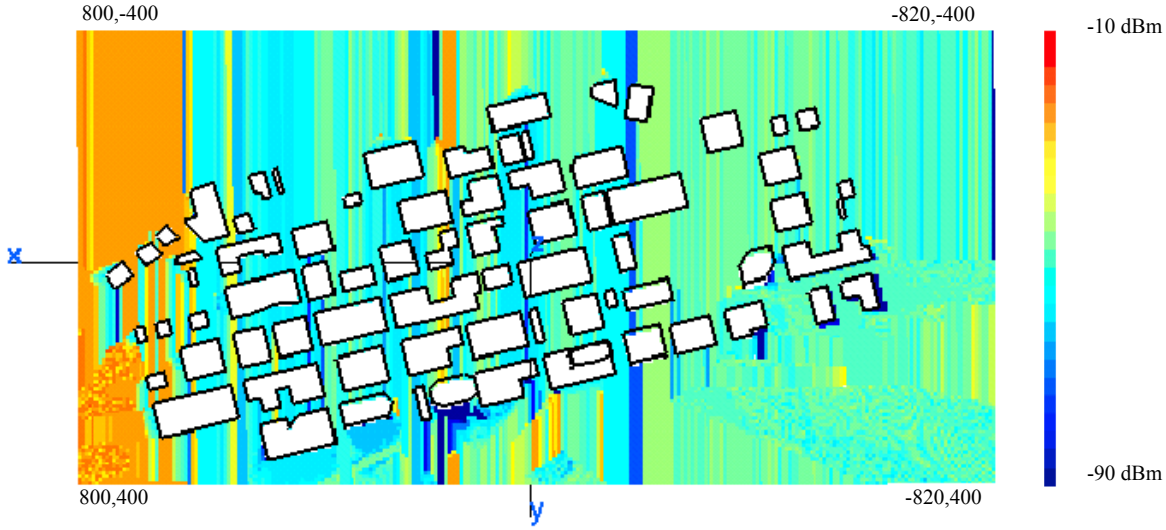

Figure 33. Two UAVs transmitting with a phase difference of π.

Comparing both figures with Figure 30, it is observed that there is an insignificant deviation in signal contours when the two UAVs were transmitting non-coherently. There were no large changes due to constructive or destructive interference of the two transmitter signals. This result negates the need for active synchronization of UAVs, which is realistically difficult to achieve and maintain.

5. Deploying Three UAVs

In this scenario, three UAVs were deployed at various locations outside the city boundary for investigation. All UAVs transmitted with the same power, frequency and were coherent in phase. In Figure 34, UAVs were deployed at the left and right sides out of the city boundary, at (53 m, −361 m, 160 m), (150 m, −540 m, 200 m) and (600 m, 400 m, 170 m). Comparing with Figure 29, it is observed that with an additional UAV, there was an improvement in radio coverage, especially in the center of the city.

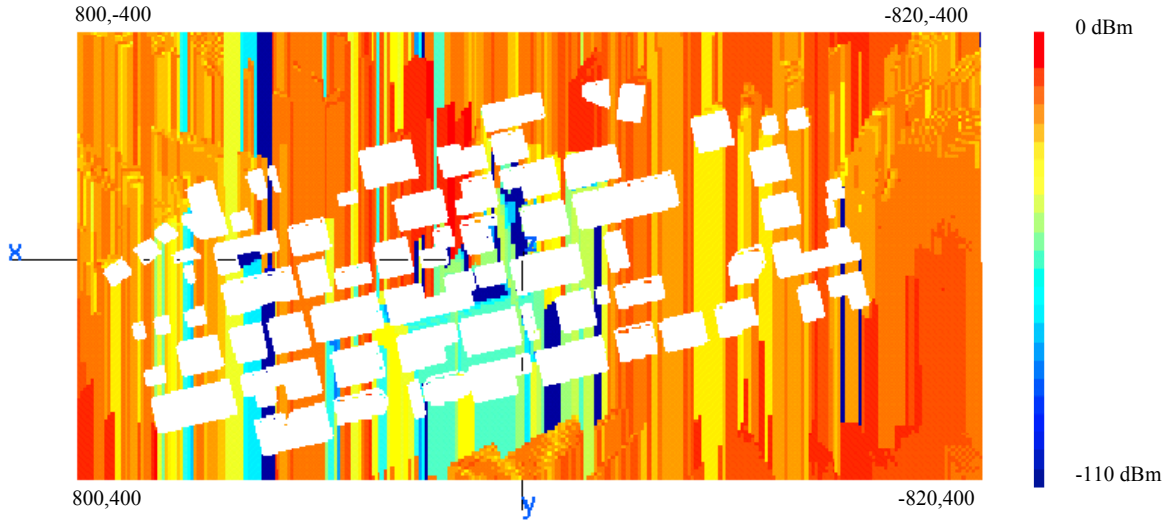

Figure 34. Three UAVs outside city boundary.

Next, three UAVs were deployed at various locations to investigate the effects on signal contours in the city. In Figure 35, in addition to the deployment of two UAVs as shown in Figure 30, a third UAV was deployed at (0 m, 50 m, 180 m).

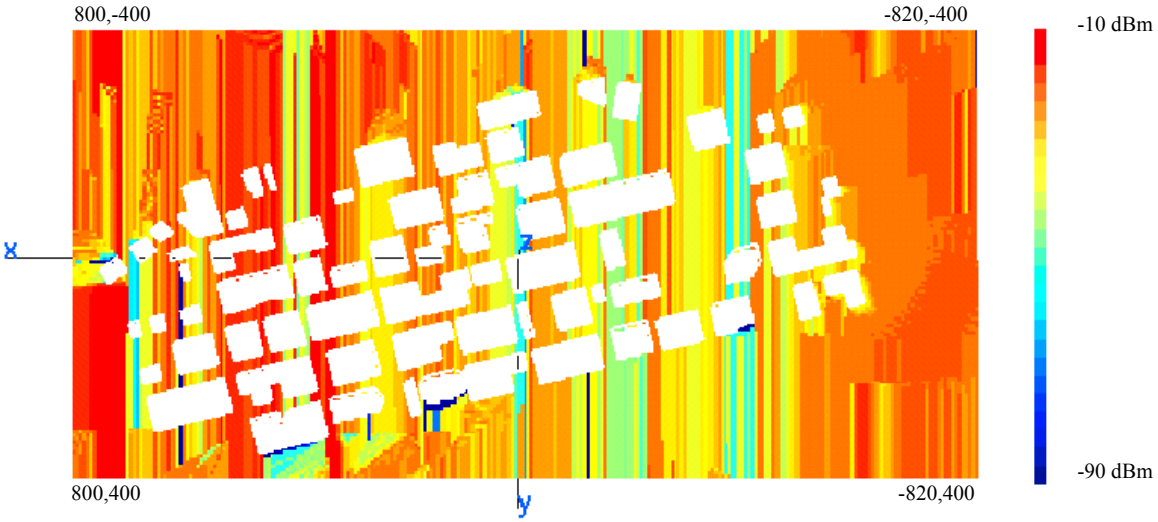

Figure 35. Three UAVs inside city boundary.

Comparing with Figure 30, it is observed that, with an additional UAV, there was an improvement in signal coverage, particularly in the center of the city. It was observed that a deployment of three UAVs versus two UAVs provided a significantly better UAV-GCS link.

6. Different Operating Altitude

In this scenario, a single UAV was deployed at various altitudes. In the first part, the UAV was placed within the city boundary. The coordinates in the x and y-axes were at the tallest building in the city (-385 m, -10 m). The z-coordinate was set at 1000 m and 10,000 m with the signal contours depicted in Figure 36 and 37, respectively.

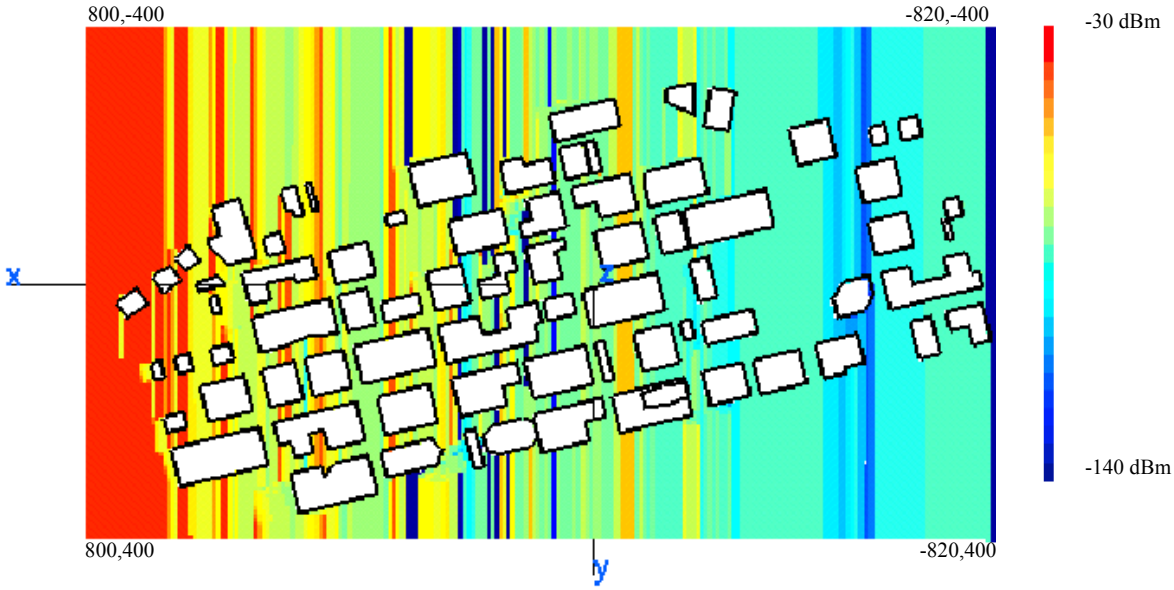

Figure 36. Varying altitude (z = 1000 m).

At three times the height of the tallest building, coverage within the city using a single UAV provided better coverage contours than using two UAVs operating at lower altitudes or perched at rooftops. A larger grazing angle creates smaller shadow areas around buildings. However, a hovering UAV at high altitude will be consuming energy during flight as compared to one that is perched at rooftops on standby mode and will require meticulous planning.

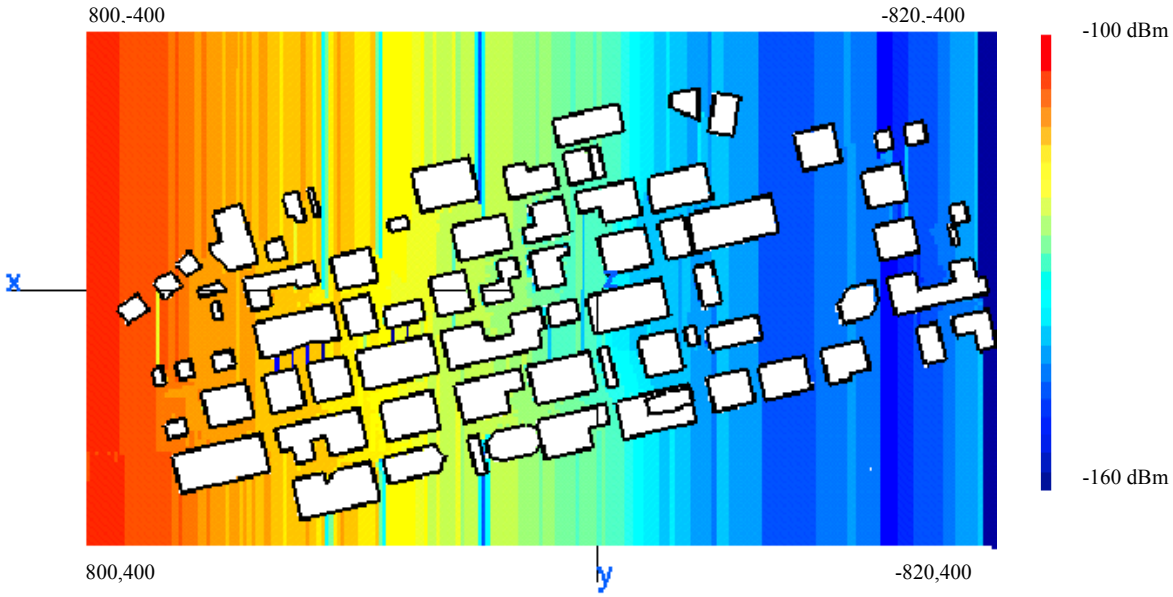

Figure 37. Varying altitude (z = 10000 m).

Figure 37 shows that, at a high altitude, the area directly under the dipole antenna will experience a null, while locations further away are in a region of higher antenna gain. Path loss increases substantially which can only be compensated by transmitting at a higher power. There was a 70-dBm drop in peak power despite an increase in operating height ratio of only 10 times. The range of power difference was 60 dB, compared to 110 dB in Figure 36. The advantage of operating at high altitude would be a larger area of uniform illumination. Requirements for adaptive positioning of the GCS would subsequently diminish.

Next, the UAV was positioned out of the city boundary. The coordinates in the x and y-axes were at (-1200 m, 377 m). The z-coordinate was set at 1000 m and 10000 m with the signal contours depicted in Figures 38 and 39, respectively.

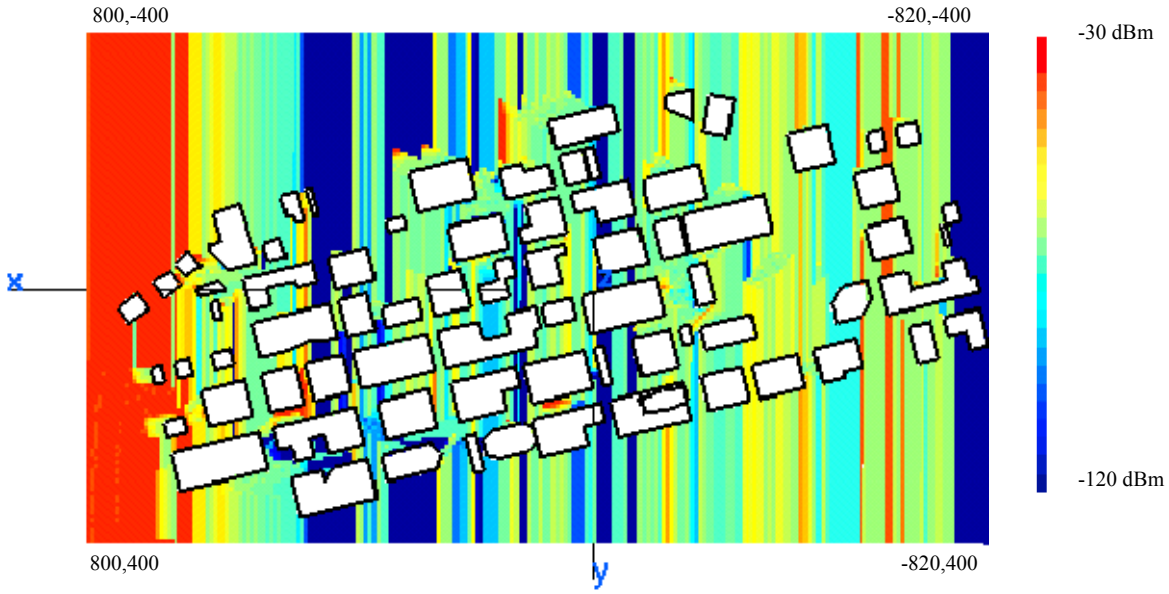

Figure 38. Varying altitude (z = 1000 m).

It is observed that the city is moderately illuminated. Regions at the left of the city, away from the UAV, receive higher signal strength. Comparing with Figure 21, it is observed that urban canyons were not created. Thus positioning of the UAV is pivotal in utilizing the urban canyon effect.

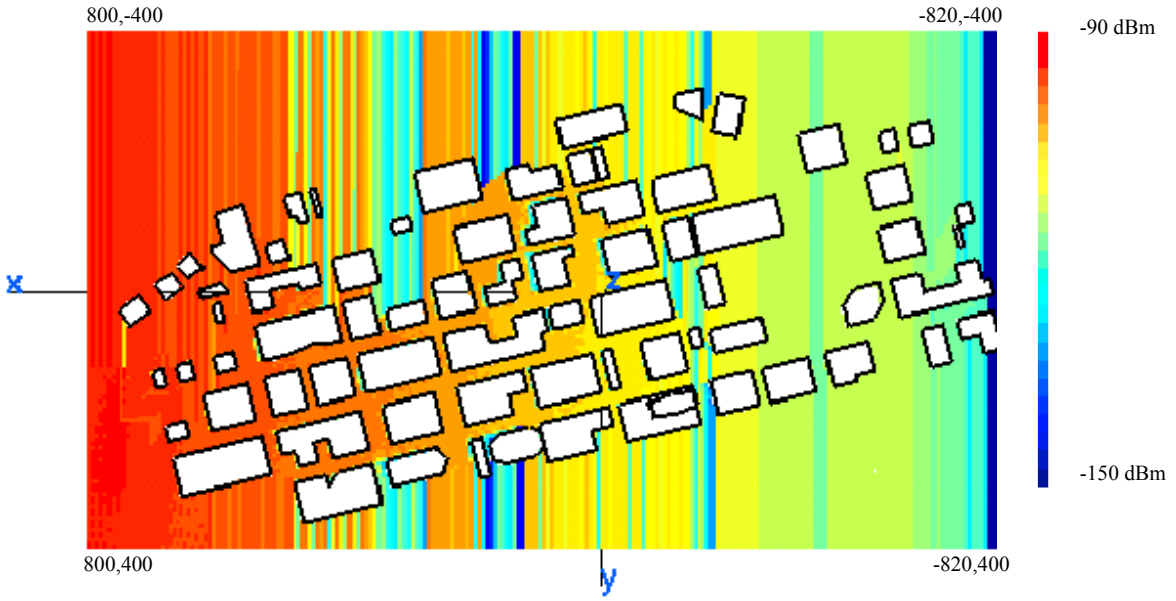

Figure 39. Varying altitude (z = 10000 m).

It is observed that almost the entire city is illuminated uniformly at around –120 dBm. Path loss is substantial due to the increase in operating altitude. Comparing with

Figure 37, there was a better signal strength level in the city. This suggests it is more efficient to operate a highflying UAV out of the target area to optimize signal coverage. Again, the range of power difference was significantly lower for a UAV operating at high altitude.

Next, two UAVs were positioned at the bottom right quadrant (250 m, 250 m, 50 m) and top left quadrant (-400 m, -400 m, 20 m) of a suburban model. Signal contours are shown as Figure 40.

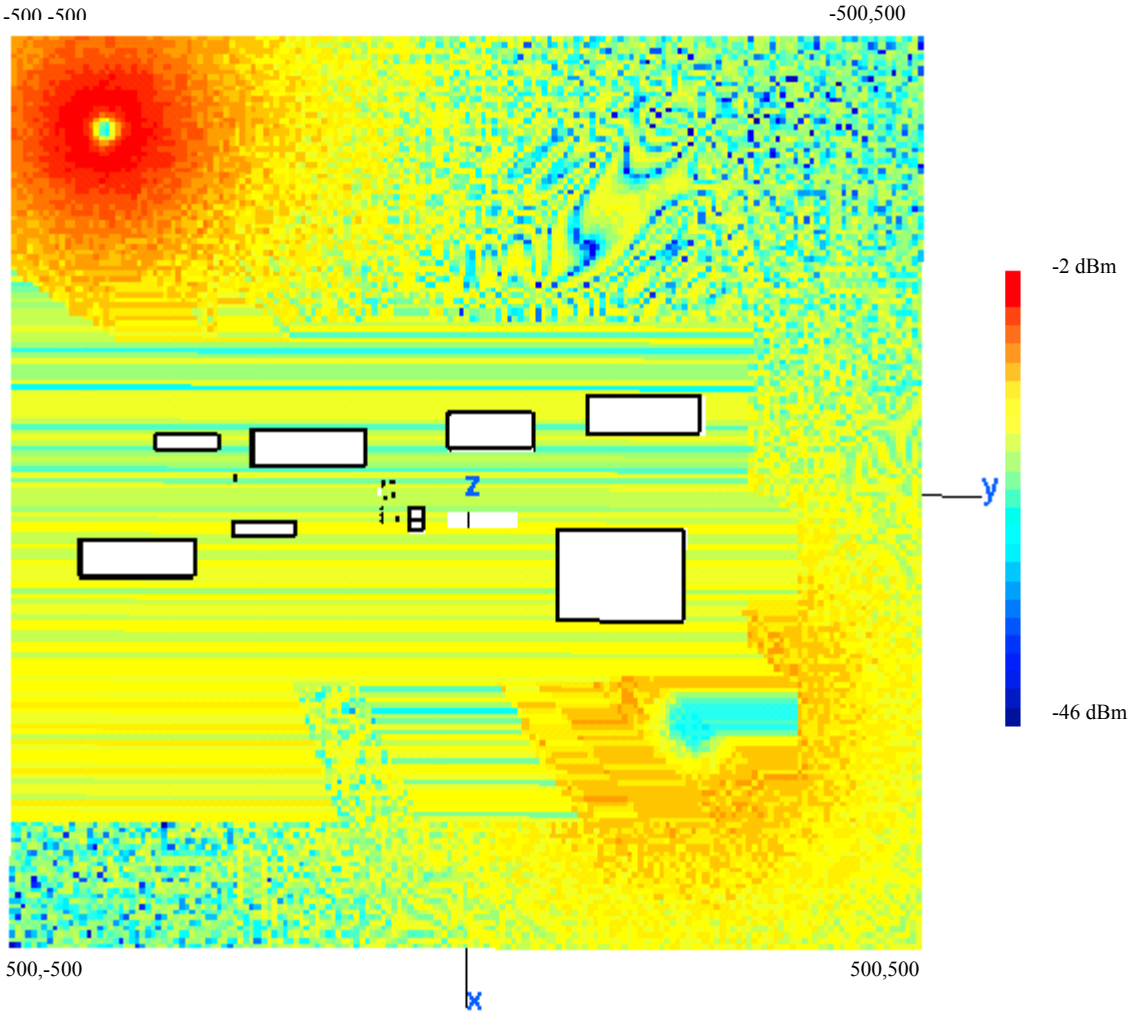

Figure 40. Two UAVs at varying altitude.

The signal contours show severe interference at top right and bottom left, possibly caused by diffraction and backscatter. Backscatter is also creating destructive interference towards the source at the bottom right quadrant.

7. Different Operating Frequency

In this scenario, the operating frequency for a single UAV was varied for investigation. The location of the UAV was modeled at the tallest building (−385 m, −7 m, 358 m). The frequency was set at 5 GHz and 15 GHz, which are typical UAV operating frequencies. The signal contours are shown in Figures 41 and 42, respectively.

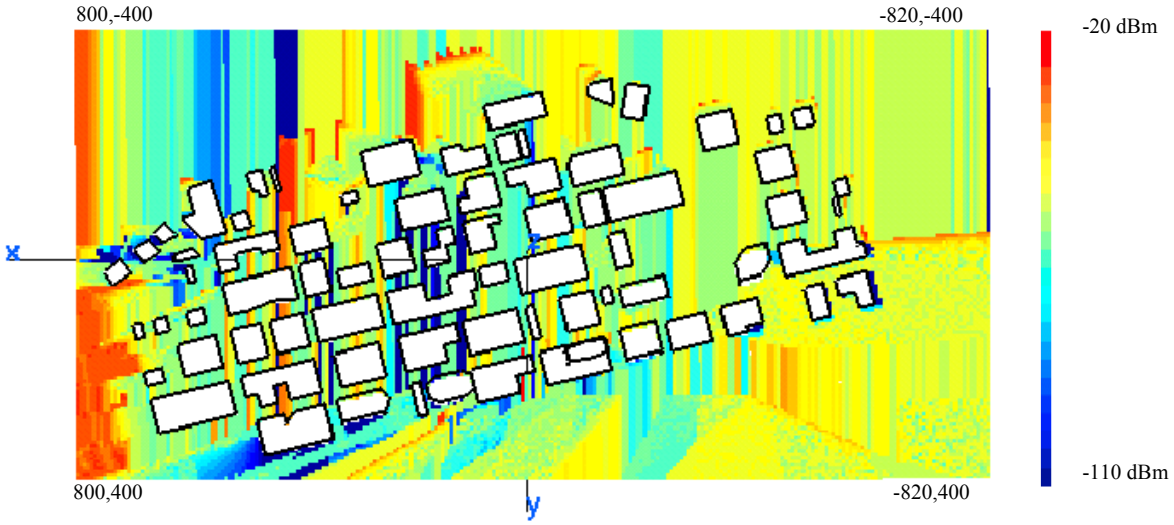

Figure 41. Varying frequency (f = 5 GHz).

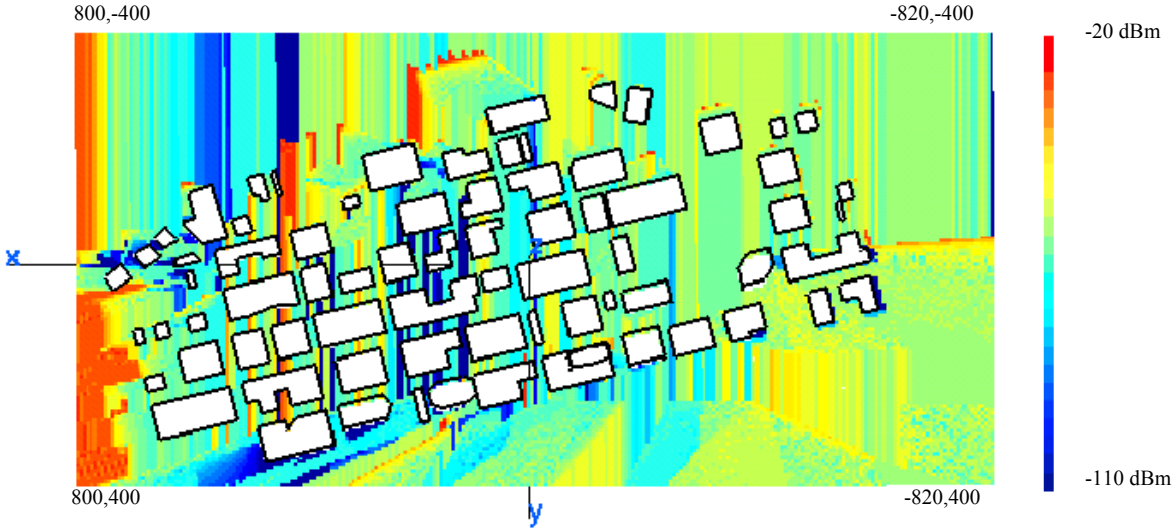

Figure 42. Varying frequency (f = 15 GHz).

Comparing both figures, it is observed that there is an insignificant deviation in signal contours if the difference in wavelength is small compared to the size of the buildings.

8. Indoor Reception For GCS

The research subsequently focused on indoor reception of RF signals, as would happen in real-life scenarios when a soldier operates an UAV with a GCS from the safety of a building. For higher resolution, all the buildings in these scenarios were done in inches.

In the first scenario, the UAV is modeled at a distance six times the width of the concrete square house at (400 in, 2550 in, 50 in). The model is shown in Figure 14. The observation plane for all the simulations was set at mid-window level. The resulting signal contours are shown in Figure 43.

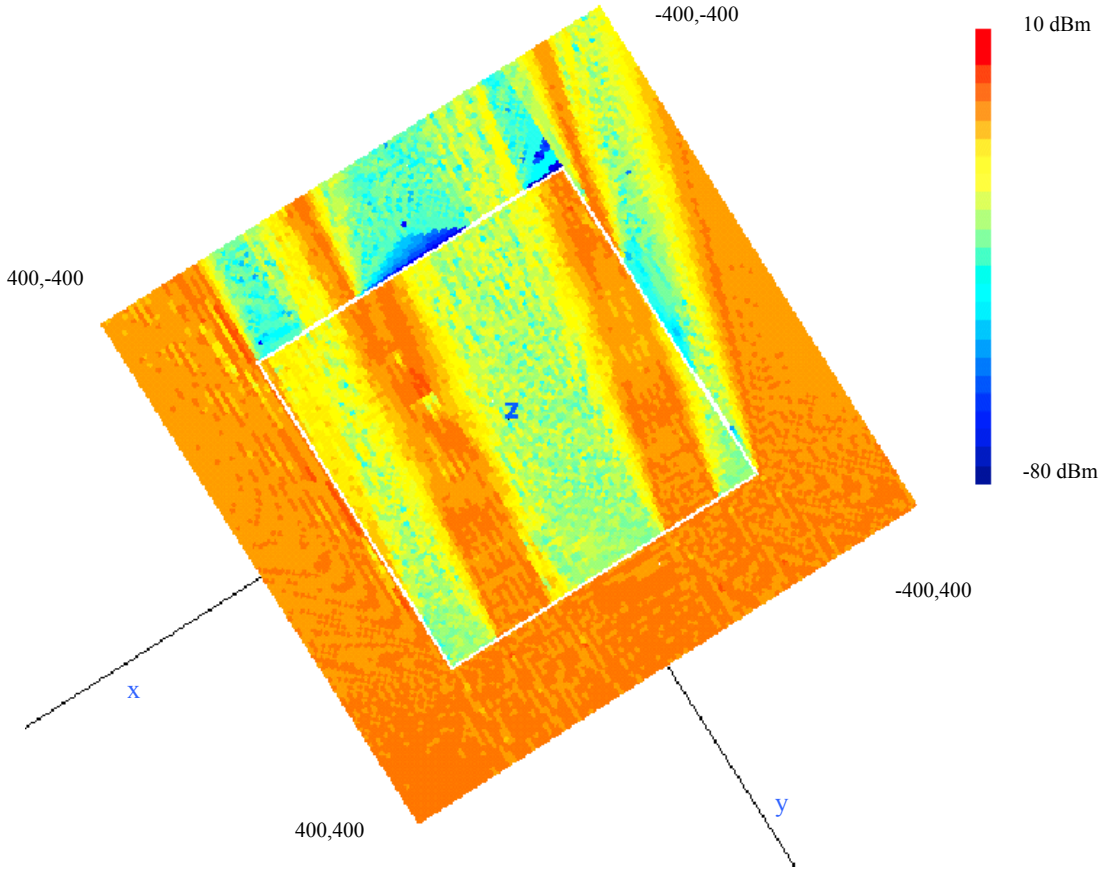

Figure 43. Single level building.

It is obvious that regions at the windows along the LOS path offer best reception. Due to diffraction at the edges of windows, regions not within the LOS path receive signals of approximately 15 dB degradation.

Next, the building model shown in Figure 15 (with a barrier wall) was used for simulation. The parameters remain the same. The resulting signal contours are depicted in Figure 44.

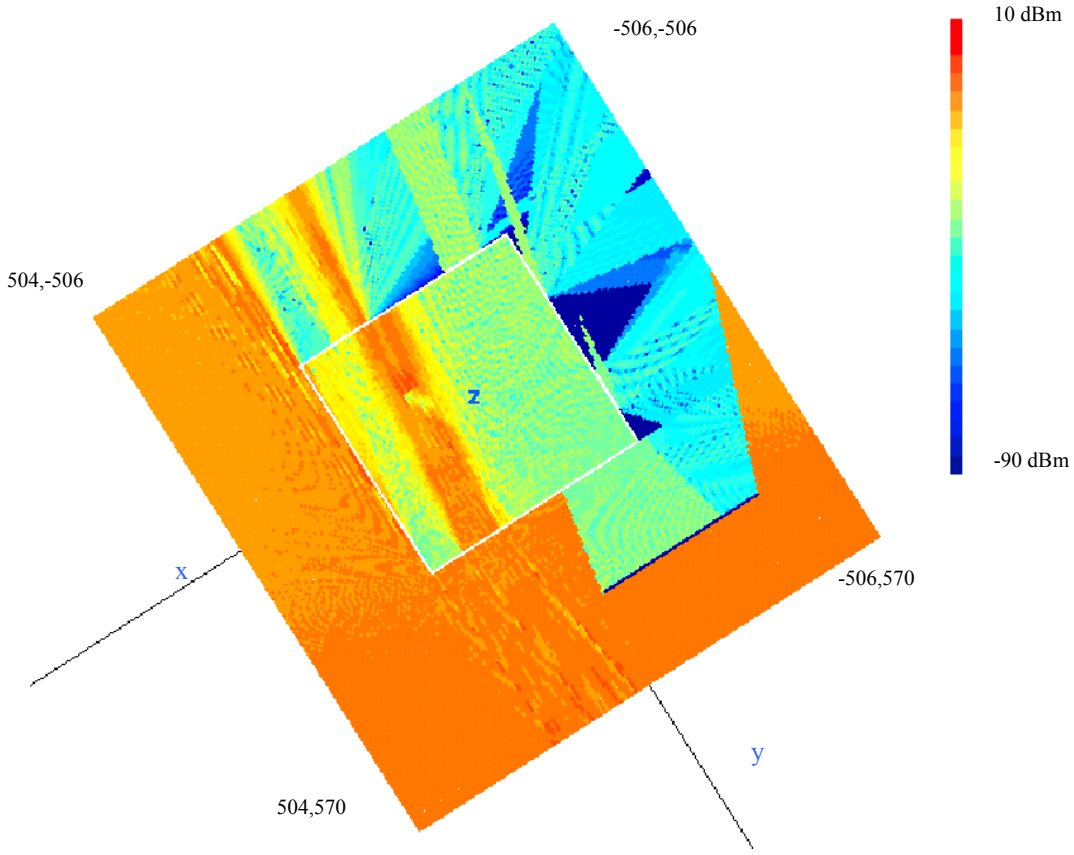

Figure 44. Single level building with barrier wall.

In this case, the barrier wall was of the same thickness as the walls of the buildings. The barrier wall effectively blocked RF signals from entering the second window. Due to multiple reflections and diffractions within the building, the region exiting the second window at the far side only drops approximately 10 dB, and is not totally shadowed. From a tactical point of view, assuming the GCS is sensitive enough to tolerate the decrease in signal strength level, it would be possible to operate at regions away from the second window to avoid visual exposure.

Next, the building model shown in Figure 16 was used for simulation. Again the parameters remain the same. The resulting signal contours are shown in Figure 45.

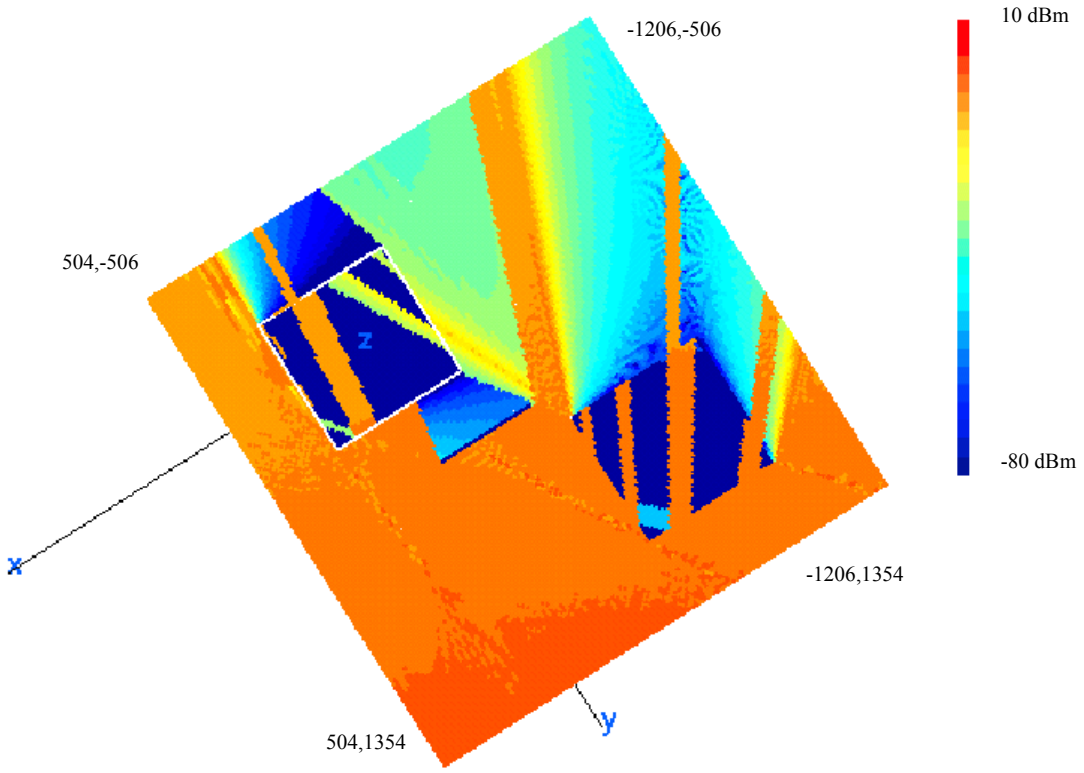

Figure 45. Two single level buildings with barrier wall (400 in, 2550 in, 50 in).

An interesting observation is that diffraction from the corner of the building at the bottom right propagates into the second building through the windows. Diffraction is visible at the top corner of the second building and at the barrier wall.

Next, the UAV was adjusted to (400 in, −2000 in, 50 in) and its signal contours computed and shown in Figure 46. It is observed that diffraction at the edge of the barrier wall allows RF signals to propagate into the building at the bottom right through windows.

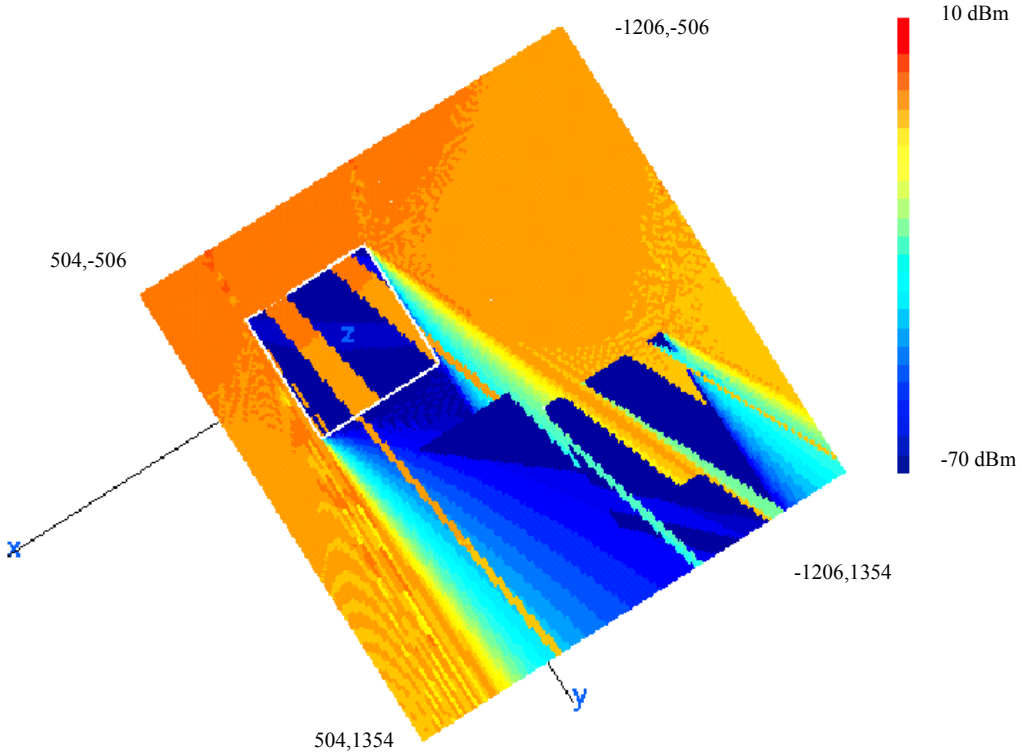

Figure 46. Two single level buildings with barrier wall (400 in, −2000 in, 50 in).

Figures 45 and 46 demonstrated the importance of diffraction in RF propagation in urbanized areas. As there are numerous edges in urbanized areas, adaptive exploitation of diffraction allows troops to control UAVs via GCS from behind windows, corners under cover from enemy fire.

For the next scenario, the building model in Figure 17 was used for simulation. Roofs were modeled as concrete with three times the thickness of the walls to minimize penetration. A single UAV was modeled at a height that is twice the height of the house at top left (−954 in, −506 in, 250 in) and bottom right (504 in, 354 in, 250 in), respectively. The resulting signal contours are shown in Figures 47 and 48, respectively.

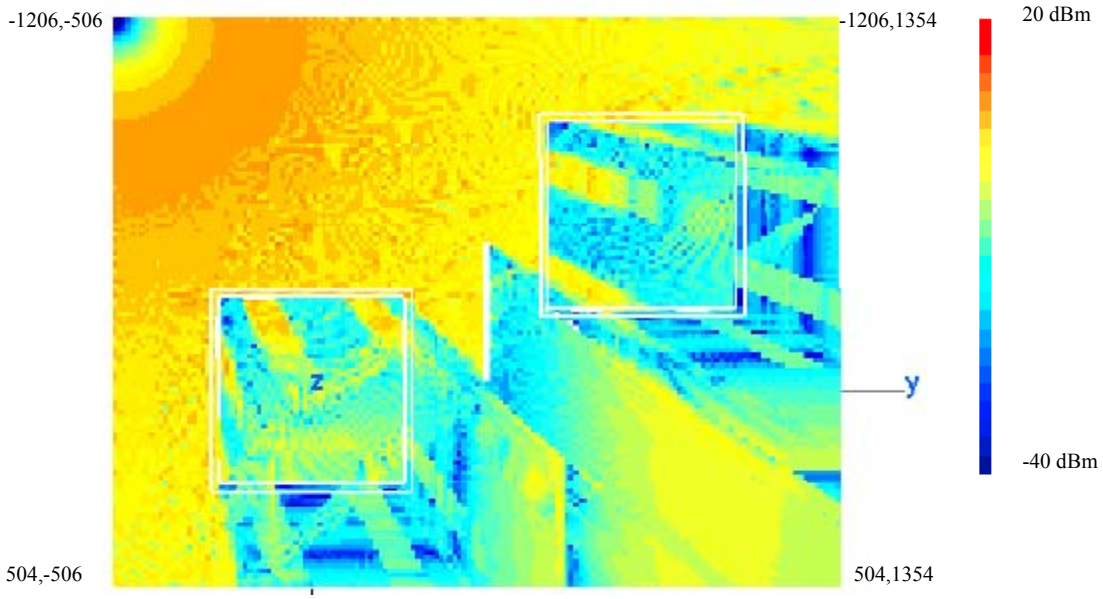

Figure 47. Two houses with barrier wall (−954 in, −506 in, 250 in).

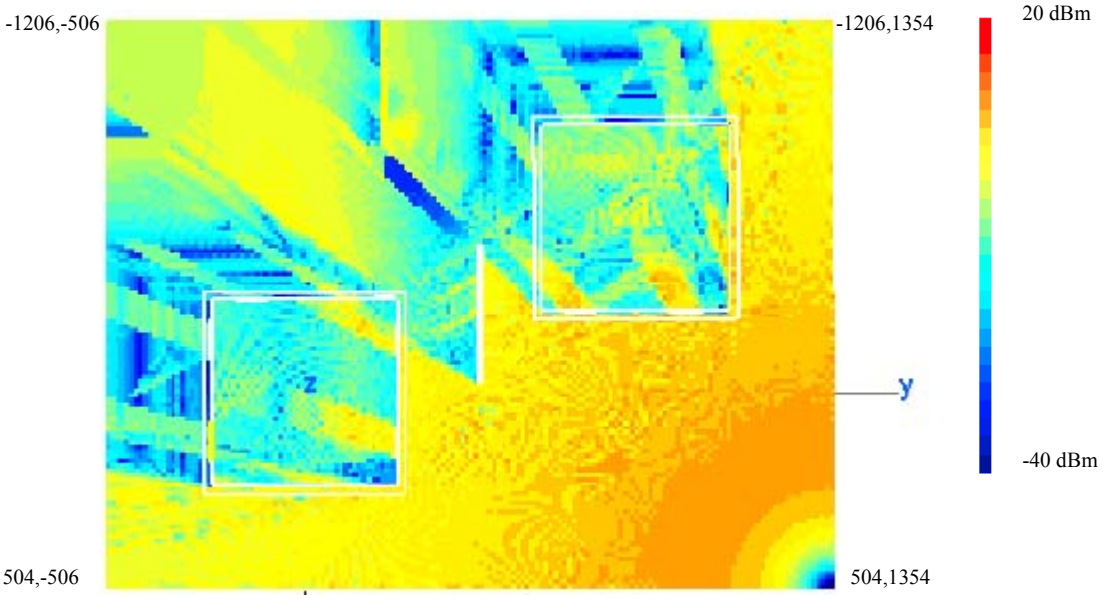

Figure 48. Two houses with barrier wall (504 in, 354 in, 250 in).

It is clearly seen from both Figures 47 and 48 that the presence of walls and roofs prevents penetration of RF signals. The only avenue will therefore be openings such as windows and doors.

Next, the UAV was located above the lower edge of the barrier wall at 2 and 3 times the height of the house. Its signal contours are depicted in Figures 49 and 50, respectively.

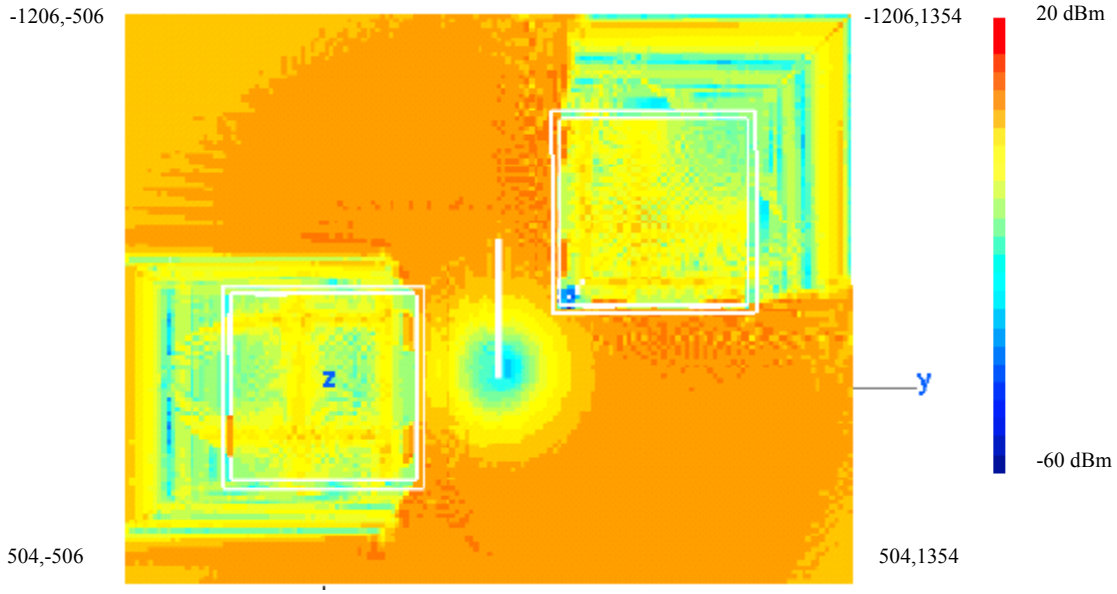

Figure 49. Two single level buildings with barrier wall (–50 in, 450 in, 300 in).

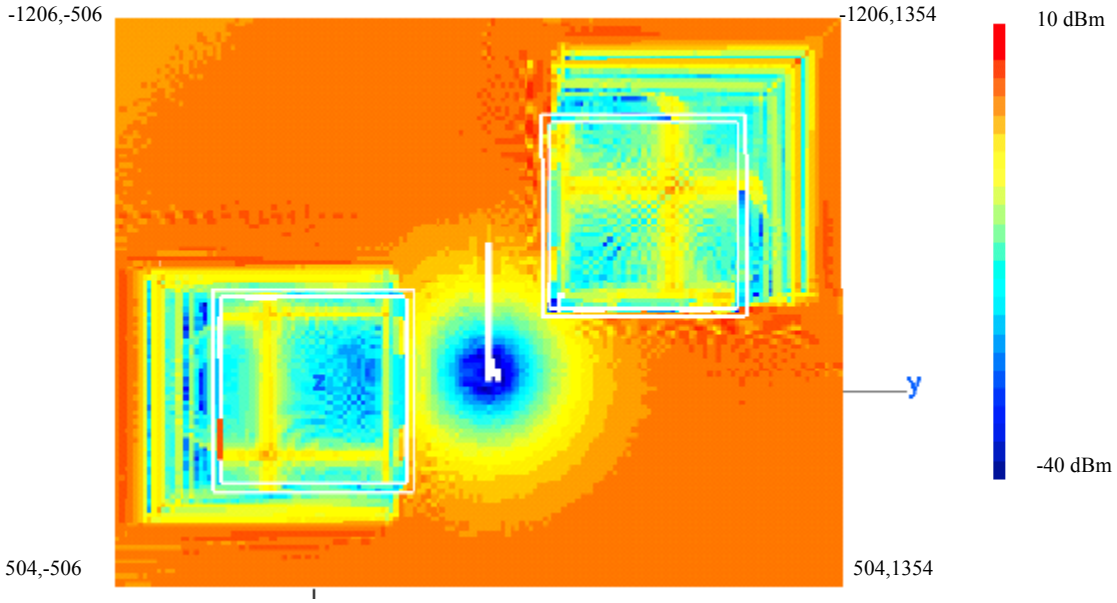

Figure 50. Two single level buildings with barrier wall (–50 in, 450 in, 400 in).

Comparing both figures, a one-third increase in the altitude changes the contour significantly. In terms of signal strength level, reception in all of the houses was maintained above –15 dBm. In Figure 50, the top right house experiences a unique contour pattern. Instead of a pattern with stronger regions at windows, multipath inside of the building created a cross-like pattern with a strong signal level at the intersection. In

this configuration, troops are able to operate an UAV away from windows in the middle of the house.

Next, the UAV was modeled at the top of the house at the bottom left. The altitude was modeled at 3 times the height of the house. Its signal contours are depicted in Figure 51.

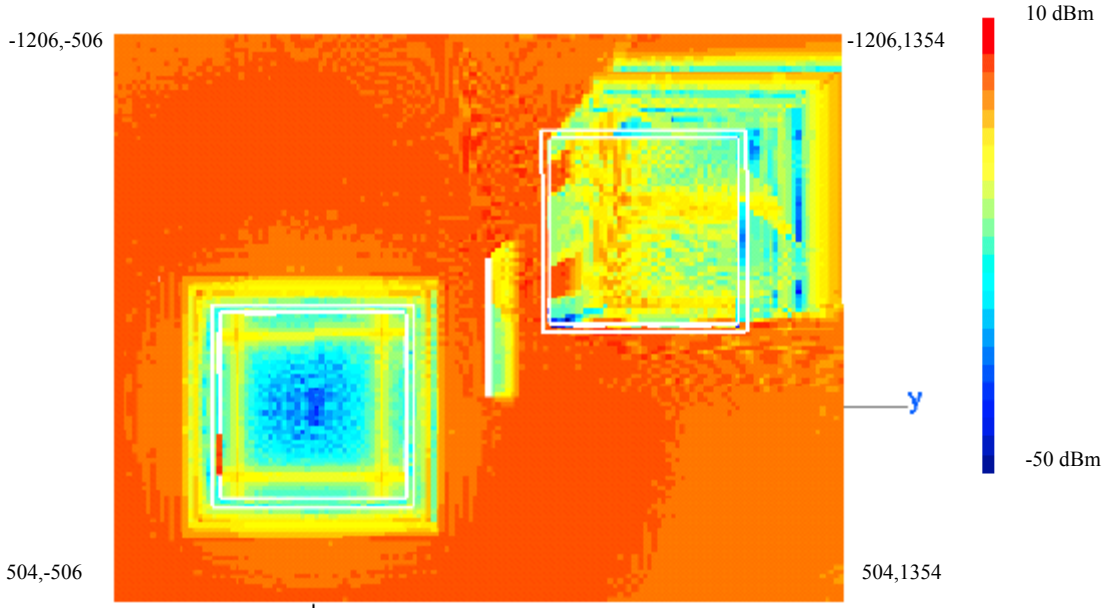

Figure 51. Two single level building with barrier wall (0 in, 0 in, 400 in).

Since the roof prevents penetration, the signal contour in the bottom house can only be caused by diffraction from the edge of the roof and propagating through the windows. The shadow region in the house was observed to change with altitude.

9. Zoom In

In this scenario, the UAV was modeled at (400 m, 400 m, 50 m). By changing the *filename.obv* file, two separate *filename.list* files were created thus allowing to view in two observation planes, namely a larger low-resolution signal contour and a smaller high-resolution image. In the latter case, areas around the buildings were zoomed into for analysis. This higher resolution would show the small-scale interference features.

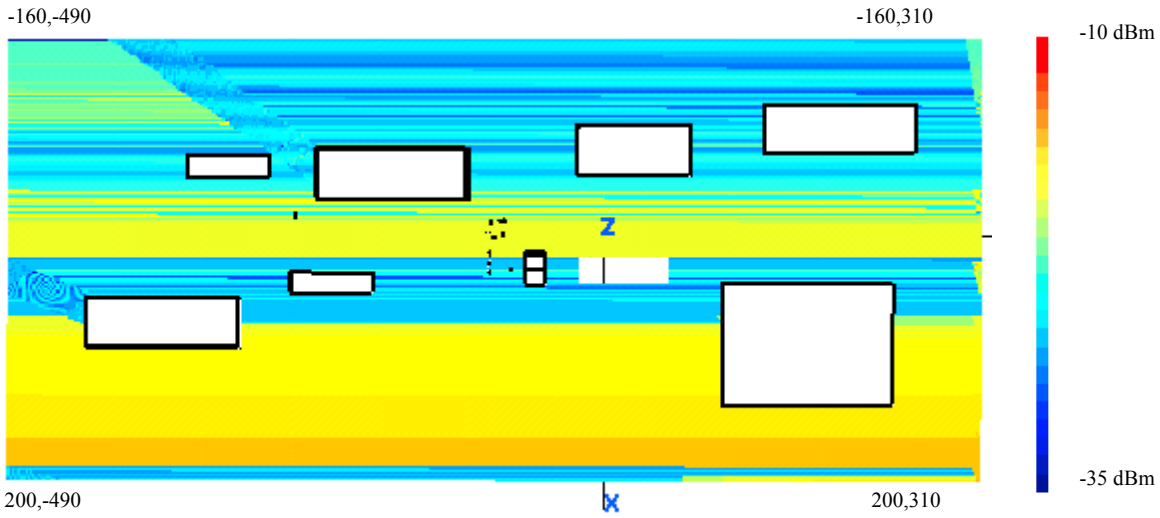

Figure 52. Low-resolution signal contour with footprint size of 2 m × 2 m.

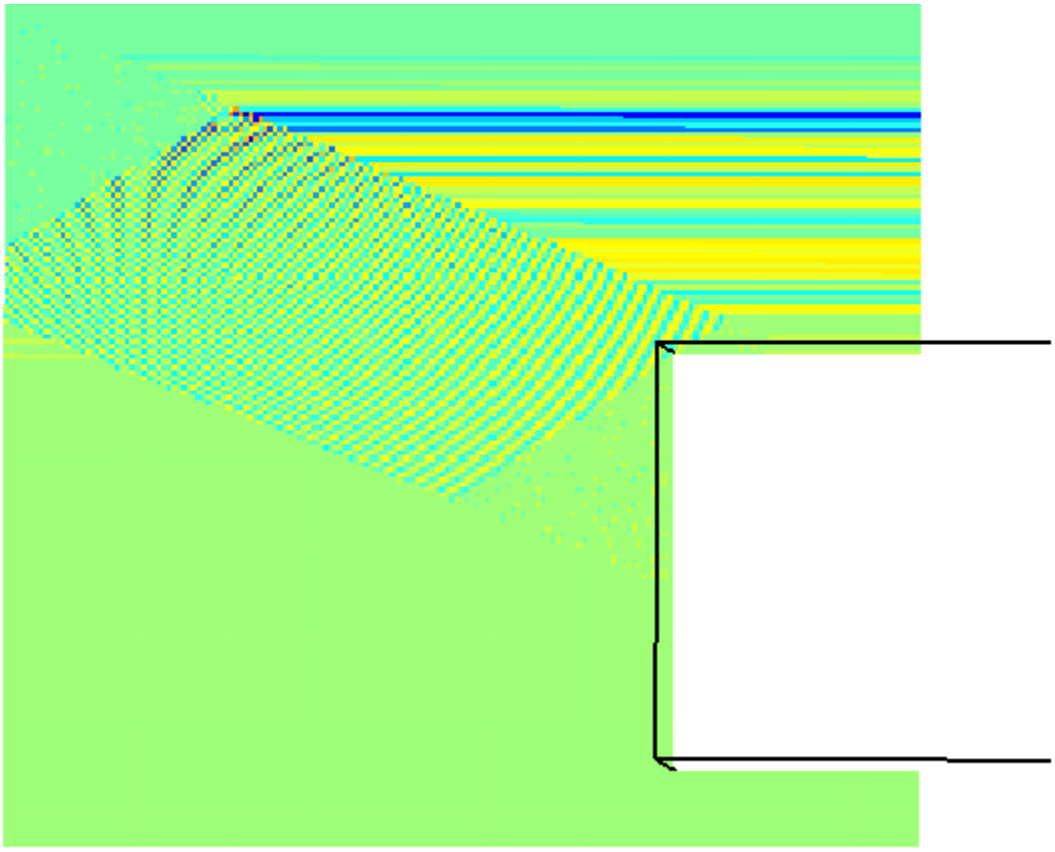

Figure 53. High-resolution signal contour with footprint size of 0.5 m × 0.5 m.

Comparing Figures 52 and 53, a higher resolution of the signal contour can be obtained using a smaller footprint of sampling space, in this case a footprint size of 2 m × 2 m versus 0.5 m × 0.5 m. Diffraction pattern off the edges of the building at the bottom level was clearly visible in Figure 53.

10. Material Coatings

A dielectric material is a substance that is a poor conductor of electricity, but an efficient supporter of electrostatic fields. In practice, most dielectric materials are solid. An important property of a dielectric is its ability to support an electrostatic field while dissipating minimal energy in the form of heat. The lower the dielectric loss (the proportion of energy lost as heat), the more effective is a dielectric material. Another consideration is the complex dielectric constant represented by $\varepsilon = \varepsilon' - j\varepsilon''$, and the extent to which the material attenuates EM waves. Dielectric loss increases with the imaginary part ε''. Substances with a low dielectric constant include a perfect vacuum, dry air, and most pure, dry gases such as helium and nitrogen. Materials with moderate dielectric constants include ceramics, distilled water, wood, and glass. Metal oxides, in general, have high dielectric constants.

Resistivity R_s is the factor in the resistance that takes into account conduction current loss in the material. Materials with infinitely large R_s can be treated as "transparent" with a reflective coefficient, $|\Gamma| = 0$ while those with small R_s are highly reflective or a $|\Gamma| \approx 1$.

In this scenario, the material of the walls in the city was modeled as concrete, glass and wood of the same thickness. The values of thickness, dielectric constant and resistivity are shown as Table 3. In **Urbana**, "transparent" materials can be represented by a resitivity value of 1×10^{30}.

Material	Thickness (m)	$\varepsilon', \varepsilon''$ (F/m)	R_s (Ωm)
Concrete	0.3	10, 51.4	1×10^{3}
Glass	0.3	4, 0	1×10^{30}
Wood	0.3	3, 0.67	1×10^{30}

Table 3. Parameters for material slabs with air backing.

It is likely that the main material of the walls in the city is determined by its usage. For example, military installations will be mostly made of reinforced concrete, commercial buildings will have a large proportion of glass (as windows for aesthetic purpose) and suburban areas will have a higher proportion of wood. The UAV is modeled at the open area near the right portion of the city (-353 m, -69 m, 187 m) and the signal contours for concrete, glass, and wooden cities are shown in Figures 54, 55 and 56 respectively.

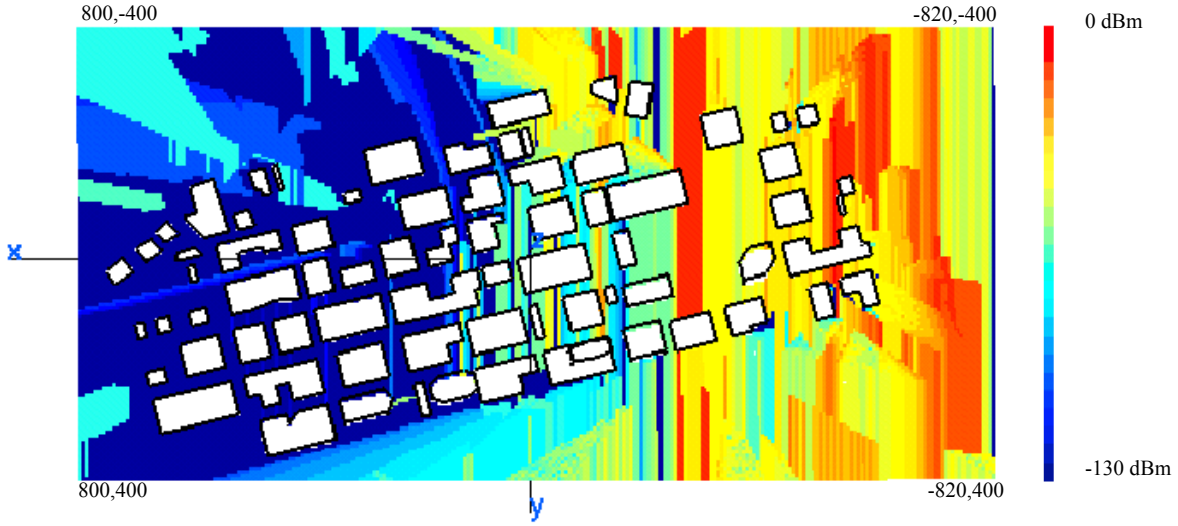

Figure 54. City with concrete buildings.

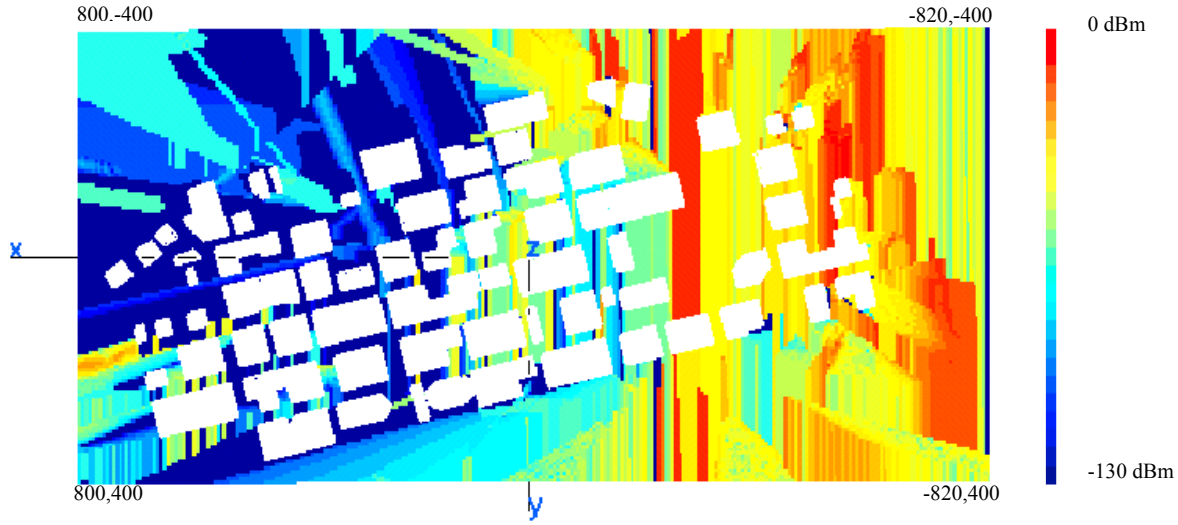

Figure 55. City with glass buildings.

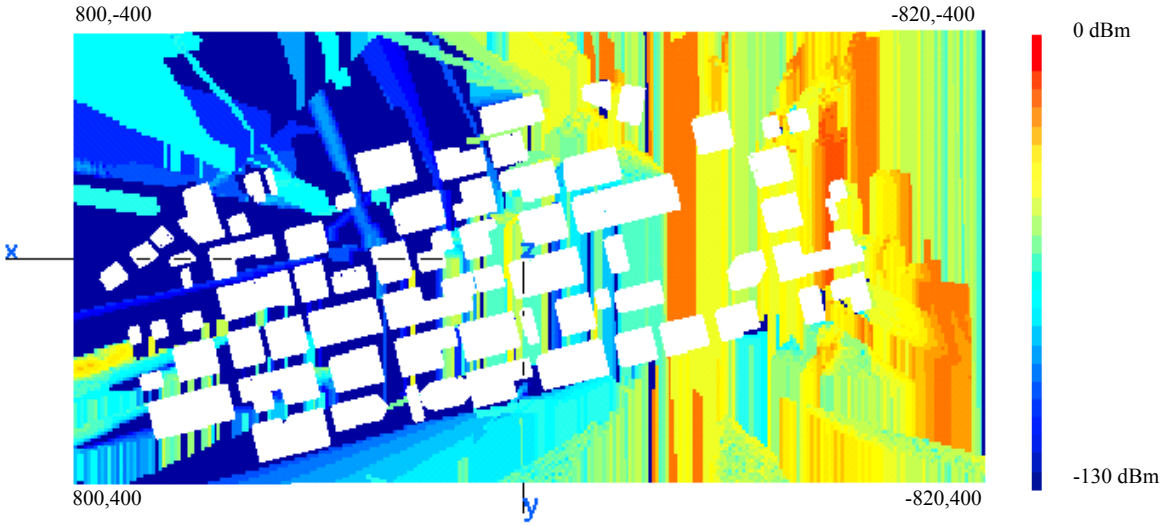

Figure 56. City with wood buildings.

The results clearly indicate that material coatings have a strong effect on the signal contours. Resistivity plays a more important role than the dielectric property of the coating. In the concrete model shown in Figure 54, propagation is limited to the open areas with large regions being shadowed. However, in Figures 55 and 56, due to a higher resistivity of the material, propagation of RF signals is more extensive.

11. Line Path

This scenario uses the same parameters used for Figure 55. The *filename.obv* file was amended to create an observation path. The aim of this simulation was to determine the fluctuations in one of the identified urban canyons in the city. The signal contour is shown in Figure 57 while a graph of signal power versus distance is plotted in Figure 58.

Figure 57. City with glass buildings with observations along a line path.

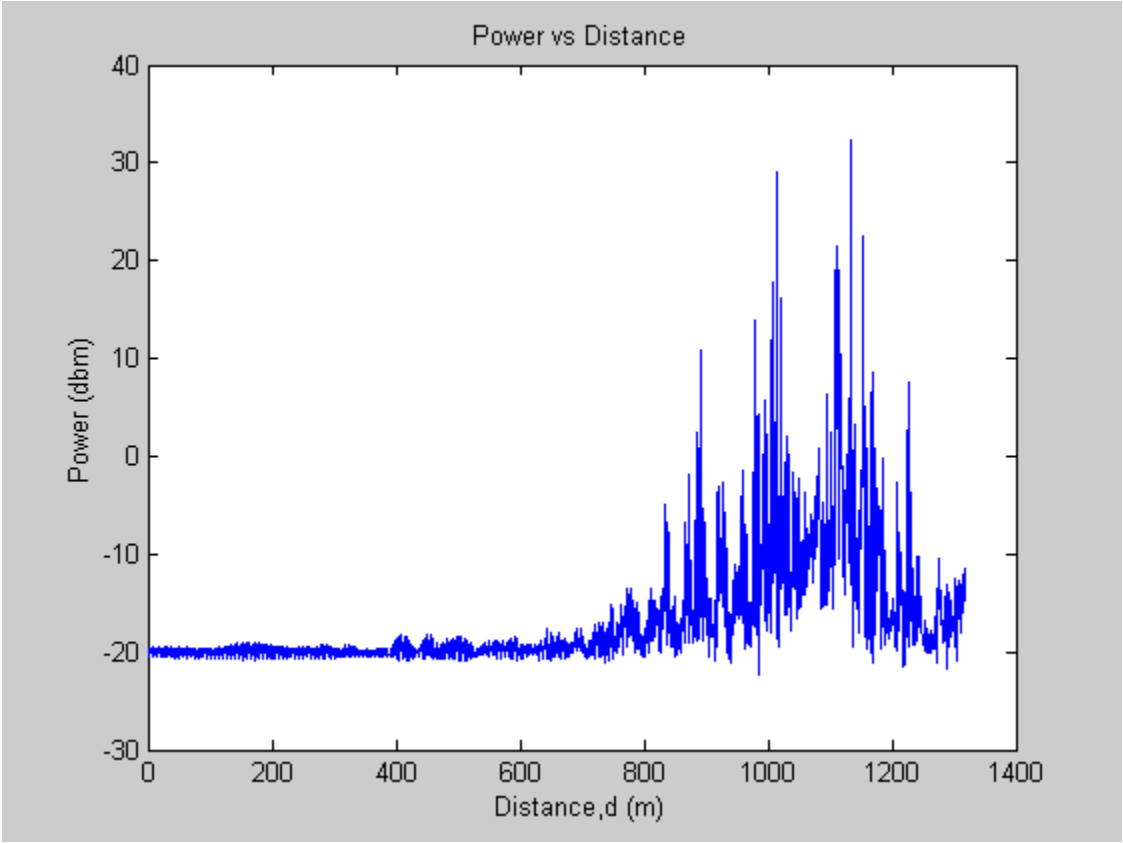

Figure 58. Power distribution versus distance.

It is observed that signal strength drops rapidly by about 50 dB within a 250-m radius but, thereafter, remains relatively constant within the canyon. The drastic drop and

presence of a second peak at 100 m away from the source is likely due to interference by the surrounding buildings.

D. SUMMARY

A majority of the simulations were run using a facet file representing a central city area. Numerous buildings and structures of irregular heights provided an insight on real-life RF propagation in urbanized areas. All of the objects were modeled in full scale and represented in either meters or inches.

This research focused on the signal contours generated when UAVs transmit omni-directionally towards an urbanized target area. The effects of varying operating frequency, altitude, transmit signal phase, material composition of building structures, and the number of deployed UAVs on the signal contours were presented. Different scenarios regarding indoor GCS reception were also presented.

IV. SUMMARY AND CONCLUSION

A. SUMMARY

Because of the growing trend towards urbanization, future wars may no longer be fought on large expanses of open terrain like pastures and deserts, but in built-up areas. At the same time, the trend towards network centric warfare puts a high demand on battlefield comprehensive awareness for commanders and troops linked by communication and sensor nodes. Deploying UAVs as ACNs, as shown in Figure 59, offers an avenue for exploitation.

Figure 59. Deployment of MSSMP (From Ref. [26].).

This research investigated the propagation of RF signals through an urbanized area using **Urbana**. Several scenarios were developed to approximate actual operational situations. Variations in the simulation included observation points, material facet composition, operating altitude, operating frequency, and theoretical ray bounce considerations.

UAV-GCS linkage in an urbanized area is subjected to multipath interference due to reflection, diffraction and scattering. Absorbing materials, corners of buildings, and windows can cause large fluctuations in the signal. Shadow regions are formed when

areas are blocked from RF signals. Severe multipath can result in a complete loss of command signals, which can limit the operational area or even cause a loss of the vehicle. However, diffraction at corners causes illumination behind walls, below towers, and spreading through small apertures, which actually helps in extending propagation.

This research focused on the signal contours generated when UAVs transmit omni-directionally towards an urbanized target area. The thrust of the research was to determine the effects of varying operating frequency, operating altitude, material composition of the building structures, and number of deployed UAVs on the signal contours. The signal strength level required to establish a link will depend on the receiver sensitivity of the GCS. There are positions outdoors and inside buildings that can satisfy the minimum signal strength requirements and they are easily identified by the color contours.

The simulation results indicate that in order to adapt to the dynamic propagation environment, an UAV deployed for MOUT must have the inherent capability to hover or fly at low speeds. Upon arriving at the pre-determined ideal location, the UAV will subsequently remain in situ for maximum coverage.

Operating at high frequency has merits of higher data rate transfer, which is crucial to support the large quantity of voice and live video feeds to be transmitted via UAV-GCS linkage. However, high frequencies are attenuated more rapidly in lossy materials like cement and glass commonly found in urbanized areas. At the same time, higher frequencies are more susceptible to attenuation due to weather like rain and fog. Having a shorter operational range translates to a smaller RF spread radius, and thus lowers the susceptibility to detection and jamming.

This research shows that there exists an optimal operating altitude of UAV for signal coverage. Perching at rooftops to minimize power consumption may not be ideal, as most of the RF waves will simply be reflected upwards. If the UAV is positioned too high above buildings, the areas beneath the UAV will experience a null when using a vertical monopole antenna and, consequently, the power received by the GCS will be diminished.

Common materials found in urbanized areas range from insulators like wood and glass, to conductors like aluminum and steel. The thickness, conductivity and permitivity of different structures determine the propagation of incident RF waves. Waves can be reflected away from structures or transmitted through with attenuation. By varying the material composition, the occurrence of urban canyons could be identified and exploited.

In summary, from analyzing signal contours, planners for MOUT will be able to provide continuous, uninterrupted and constant signal linkage between all the nodes (troops, artillery, planes, ships, sensors, etc). Using UAVs as ACNs will allow the edge in information dominance.

B. CONCLUSION

This research has established the process that can be used to predict the signal levels in an urban environment. Detailed modeling of the buildings of interest is required for an accurate prediction of the signal contours since the signal contour prediction by **Urbana** will only be as good as the accuracy of the information provided. Moreover, the software does not take into account the mobility of objects in the models and natural attenuation due to atmospheric conditions like rain and fog.

Urbanized areas are made up of mostly straight roads lined with buildings. Through simulation, the locations of urban canyons can be identified and exploited for usage. Meanwhile, identified shadow regions can either be avoided or illuminated by deploying ACNs. A single UAV operating a three times the height of the tallest building in the central city was found to provide a concentric, uniform signal coverage. This research also demonstrated that a network of low-powered UAVs provides better coverage than a single high-powered UAV.

A UAV at an ideal location would service a bigger area, which translates to a lower transmitted power and also decreases its susceptibility to detection and jamming.

Material coatings of building structures were found to play an important part in propagation. The simulation using concrete, glass, and wood as materials for the walls illustrated this point.

Due to its radiation distribution pattern, a UAV mounted with a vertical dipole, as shown in Figure 60, will have a null at areas directly below. This point was clearly shown in the simulation involving operating a UAV at high altitude, and illustrates the need for other alternatives for the main transmitting antenna.

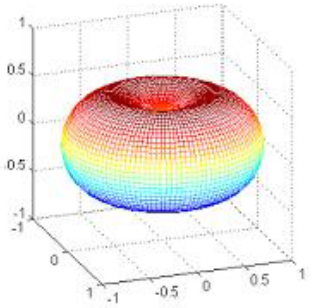

Figure 60. Spatial radiation distribution of a vertical dipole antenna.

Future work might include the investigation of UAV-GCS linkage in the presence of jamming, simulations involving directional antennas, comparison of predicted signal contours with physical measurements, simulations involving underground building structures and simulations with advance options. These are discussed in the following section.

C. FUTURE WORK

1. Performance in Presence of Jamming

Smaller UAVs may not be capable of frequency hopping and advanced frequency modulation techniques due to its inherent limited payload. Consequently, they are highly susceptible to wide-band jammers. Effects on ground signal contours and P_r of both the UAV and GCS could be investigated.

2. Comparison of Simulated Results with Actual Physical Measurements

The presence of excellent radars and laboratory facilities at Naval Postgraduate School presents an opportunity for the actual measurements of signal contours of designated buildings. A detailed model of the school could be coded using available blueprints.

3. Simulations with Advance Options in URBANA

Advance options include a GTD blockage model for indoor propagation and a simple terrain blockage model to include diffraction due to terrain, double diffraction, and multiple diffraction. Advance options offer finer resolution for analysis.

4. Simulations Involving Underground Structures

The war in Iraq highlighted the need to locate and identify underground facilities. Research in this area might include dielectric properties of ground soil under different atmospheric conditions, transmitted peak power required, and the operating motion of surveying UAV.

5. Simulations with Directional Antennas

Advanced, large UAVs like Predator have both omni-directional antennas and directional antennas. High-gain directional antennas have small beam widths and are less susceptible to multipath interference. Effects of highly directional pencil beams hitting wedges could be a topic for further investigation.

D. APPLICATIONS TO MILITARY OPERATIONS

1. Detailed Signal Contours at Buildings of Interest

Work of immediate importance might include the detailed modeling of critical buildings of interest. Accurate information pertaining to the thickness of walls, materials used, and wedge angles of walls, is crucial to building a reliable model. Knowledge of the signal contours at the areas of interest will determine the deployment of UAVs to provide the required coverage for troops in MOUT.

2. Ground Penetrating Radar Images

Urbana can be used to create a data bank of signal contours of underground storage tanks (USTs), tunnels and underground command posts at various depths, conductivity of ground, and thickness of walls. The data bank will add resolution to the accuracy of ground penetrating radar (GPR) images.

3. Susceptibility to EM Detection by UAV

Future command posts will mostly be underground made of thick reinforced concrete as shown in Figure 60. This research has shown that any opening in the structure will allow emission of RF signals. Thus models of command posts could be created using **Xcell** and, using the "Receive-antenna" feature in **Urbana**, determine the power received by the UAV. The result of the simulation can be readily used to enhance the security of a command post by employing the necessary ECM techniques.

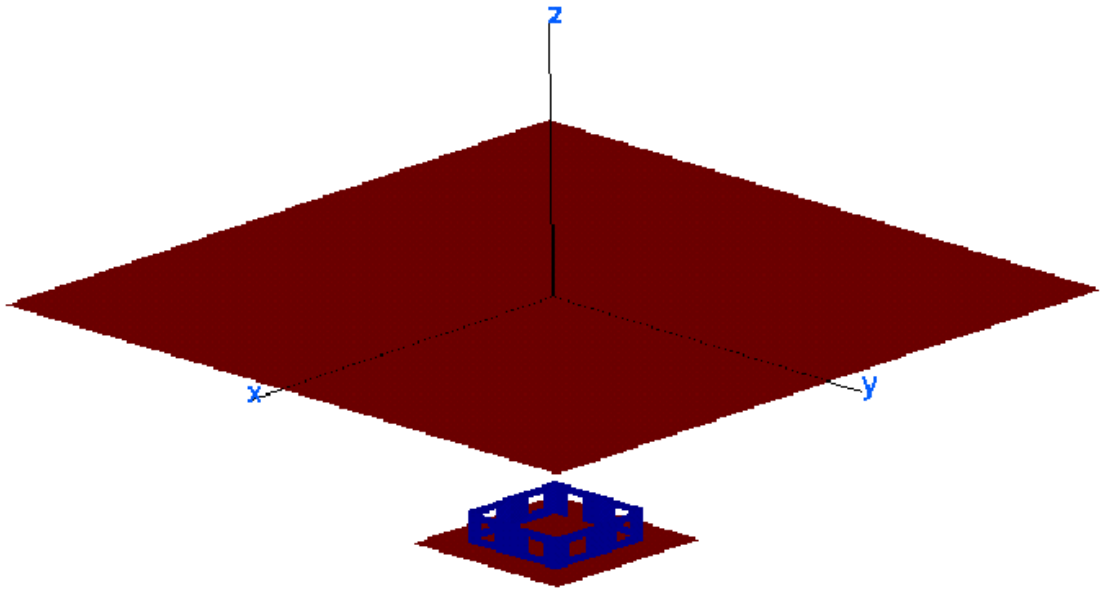

Figure 61. Underground command post.

APPENDIX

A. URBANA INPUT SCRIPT FILE

The following is a listing of a typical **Urbana** input file *filename.ur_input*:

```
        --- input Urbana v 2.5
#
# ********************************
# A---scatterer file,length & freq
# ********************************
#--- name of scatterer file in ACAD format (e.g. wall.facet)
filename.facet
#--- length unit:1=inch, 2=cm, 3=meter, 4=mm, 5=mil
3
#--- uniform freq (GHz): start freq, end , nstep
#    (nstep=0 means: just do first freq. CAUTION: antenna patterns are
#     assumed to be indep. of freq and is calculated at end freq)
5 5 0
#
# *********************************
# B--- Antenna Description and List
# *********************************
#
#---Enter method of describing antennas.
#   (1 = here, 2 = file):
1
#---If described in file, enter file name:
dummy.antenna
#---If described here, fill in sections B1, B2, B3.
#   If described in file, use dummy data in sections B1, B2, B3
#   (specify one dummy antenna type, dummy antenna origin,
#    and one dummy item in antenna list).
#
# ************************
# B1: Define Antenna Types
# ************************
#
#   Two lines for each type.
#     Line1: type ID, ant code
#     Line2: parameters
#
#   Type ID must start from 1 and increment by 1 thereafter
#
#   Ant Code   meaning          parameters
```

```
#   --------   ---------------   ----------------------------
#      1       pattern file       filename(ascii)
#      2       dipole             length(real)
#
#   Antenna Types list:
#
#   Enter number of antenna types:
1
#   Type #1
1 2
0.06
#
# ***********************************************
# B2: Enter origin of antenna coord in main coord
# ***********************************************
#
0.0 0.0 0.0
#
# ************************
# B3: Create Antenna List
# ************************
#
#   Three lines for each antenna.
#     Line1: Type ID, location (x,y,z), power (watts), phase(deg)
#     Line2: Local x-axis in main coord.
#     Line3: Local z-axis in main coord.
#
#   Enter number of antennas:
1
#
#   Antenna #1
1  400.0 –7.0 358.0  1. 0.
1. 0. 0.
0. 0. 1.
#
# ***********************
# C---Observation points
# ***********************
#--- Observation points defined with respect to main coord. system 7.
#    Enter method of specifying list of points.
#    (1 = here, 2 = file):
2
#--- If points are listed here, enter number of points (kobtot):
1
#--- If listed here (1 above), List xyz of points in main coord 7
#    (one point at a line). If 2 above, include one dummy line.
```

```
1.          2.          -11.00
#--- If points listed in file (2 above), enter name of file.
filename.list
#--- Include direct Tx to observer contribution.
#   If you turn on the direct contribution from the transmitter to the
#   observation point, computed result will be the total field, which is
#   the incident + scattered field.   For propagation analysis, this is
#   the preferred setting.  Otherwise, the result only includes the
#   scattered field.
#
#   Include direct contribution from transmitter to observation point (rx)
#   (1 = yes, 0,2 = no):
1
#--- Compute received power into Rx antenna.
#   Urbana always computes field levels at the observation point.
#   If you specify an Rx antenna, Urbana will also compute the received
#   power and record the results in the (runname).couple file.
#   This causes a moderate but slow-down when using the SBR method (below).
#
#   Include Rx antenna (1 = yes, 0,2 = no):
2
#--- Rx antenna specification
#   Remaining entries in Section C can be ignored if not including
#   an Rx antenna.
#   Enter antenna type (1 = pattern file, 2 = dipole):
1
#   Each antenna type requires additional parameters.
#   List of expected parameters follows.  Choose one.
#
#   Type  Description     Expected Parameter(s)
#   1     Pattern File    File Name (e.g., beam.antpat)
#   2     Dipole          Length (in prevailing unit)
#
#   Enter parameter(s) on next line:
shdip.antpat
#--- Rx antenna orientation
#   Enter local x-axis of Rx in global coordinates
1. 0. 0.
#   Enter local z-axis of Rx in global coordinates
0. 0. 1.
#
# ****************************
# D---Theoretical consideration
# ****************************
#--- Choose method of computation
#   0 = compute fields in the ABSENCE of the scatterer
```

```
#    1 = compute fields by SBR
#    2 = compute fields by GO
2
#--- If SBR, select a PO integration scheme at bounce points
#    1 = do integration at first & last bounce points only
#    2 = do so at all bounce points (GTD formulation)
#    3 = do so at all bounce points (PTD formulation)
1
#--- Edge diffraction
#    SBR can be enhanced with PTD edge diffraction.
#    GO can be enhanced with GTD edge diffraction.
#    Add edge diffraction (0,2=no, 1=ILDC (SBR or GO), 3=UTD (GO only)
3
#--- If edge diffraction switched on, enter name of edge file
#    (e.g., wall.edge or dummy if edge not included).
filename.edge
#--- Choose method of ray launch
#    1 = by (baby) facet, achieving a uniform first bounce surface density
#    2 = uniform angular distribution (burst launch)
#    (If computation by GO, must select 2 = burst launch)
2
#--- If ray launch by (baby) facet (1 above), enter ray density:
#    # rays/wavelength (normally 5-10)
10.0
#--- If burst ray launch (2 above), enter angular interval (deg).
#    (Typically 0.25 - 2.0 deg)
2.0
#--- max permissible ray bounces (normally 5-10)
10.0
#--- max-voxdepth = max depth of BSP tree (normally 20)
#    max-voxl = max facets in each voxel(normally 10)
#    (Larger voxdepth & smaller voxl lead to faster ray tracing
#     but more computer memory)
15,10
#--- ICOAT for absorbing facets
888
#--- IQMATRIX for divergence factor
#     1 = calculated by Q-matrix
#     2 = ignored except for the spherical wave spread
2
#--- IF using Q-matrix, name target curvature file(e.g. wall.curv)
dummy.curv
#--- IPEC=1 if all pec,  =2 if coating present
2
#--- For PEC scatterer, give the magnitude of reflection coeff
#    (use 1.0 for ideal PEC, use less for rough PEC--fudging)
```

```
1.0
#--- IF PEC, the rest coating info is dummmy
#--- material reflection is done through a look-up table
#    specify the freq interval in GHz for the table e.g. 0.25
#    (dummy if input freq less than 51)
0.2
********************
E---coating material
********************
---- number of materials
     (NOT including pec, which is identified by ICOAT=0)
     (NOT including absorbing facets:  ICOAT=28 or 888)
     (If 3 material, urbana reads only ICOAT=1-3)
7   <----NCOTOT
--- for each material, identify its boundary type:
   iboundary = 1 if impedance boundary
               2 if layered slabs with PEC backing
               3 if penetrable layered slabs with air backing
               4 if penetrable FSS Tx/Refl table supplied by user
               5 if same as 2 except using freq-dep ramlib.d
               6 if antenna refl table supplied by user
               7 if layers over semi-infinite ground
for each material, given info by following the templates

^^^ ICOAT=1 ^^^^^^^^^^^^^^^^^^^^^^^^^^^^^^^^^^^^^^^^^^^^^^^^^^^^^^^^^^^^^^^^
--- iboundary
2   <----IBOUNDARY(ICOAT=1)
--- number of layers over air backing
   (1st layer is farthst fr incid field and innermost)
1
--- thick,epsilon(c),mu(c),resistivity(ohm)
10.0000 (10,-51.4) (1.0,0) 1.e+3
^^^ ICOAT=2 ^^^^^^^^^^^^^^^^^^^^^^^^^^^^^^^^^^^^^^^^^^^^^^^^^^^^^^^^^^^^^^^^
--- iboundary
2   <----IBOUNDARY(ICOAT=2)
--- number of layers over air backing
   (1st layer is farthst fr incid field and innermost)
1
--- thick,epsilon(c),mu(c),resistivity(ohm)
3.000 (15.0,-0.500) (1.0,-0.000) 1.e+30
^^^ ICOAT=3 ^^^^^^^^^^^^^^^^^^^^^^^^^^^^^^^^^^^^^^^^^^^^^^^^^^^^^^^^^^^^^^^^
--- iboundary
2   <----IBOUNDARY(ICOAT=3)
--- number of layers over PEC backing
   (1st layer is farthst fr incid field and innermost)
1
```

```
--- eta=(surface imped in ohm/ 120*pi).Special case:eta=0 for pec
3.000 (15.0,-0.500) (1.0,-0.000) 1.e+30
^^^ ICOAT=4 ^^^^^^^^^^^^^^^^^^^^^^^^^^^^^^^^^^^^^^^^^^^^^^^^^^^^^^^^^^^^^^^^^^^^
--- iboundary
7   <----IBOUNDARY(ICOAT=4)
--- number of layers over semi-infinite ground
   (1st layer is farthst fr incid field and innermost)
1
--- thick,epsilon(c),mu(c),resistivity(ohm)
2.00 (10,-51.4) (1.0,0.00) 1.e+30
--- epsilon(c),mu(c) of semi-infinite ground
(2.900,-0.14) (1.0,-0.00)
^^^ ICOAT=5 ^^^^^^^^^^^^^^^^^^^^^^^^^^^^^^^^^^^^^^^^^^^^^^^^^^^^^^^^^^^^^^^^^^^^
--- iboundary
7   <----IBOUNDARY(ICOAT=5)
--- number of layers over semi-infinite ground
   (1st layer is farthst fr incid field and innermost)
1
--- thick,epsilon(c),mu(c),resistivity(ohm)
0.120 (2.900,-0.000) (1.0,-0.000) 1.e+30
--- epsilon(c),mu(c) of semi-infinite ground
(2.900,-0.00) (1.0,-0.00)
^^^ ICOAT=6 ^^^^^^^^^^^^^^^^^^^^^^^^^^^^^^^^^^^^^^^^^^^^^^^^^^^^^^^^^^^^^^^^^^^^
--- iboundary
2   <----IBOUNDARY(ICOAT=6)
--- number of layers over air backing
   (1st layer is farthst fr incid field and innermost)
1
--- thick,epsilon(c),mu(c),resistivity(ohm)
3.000 (15.0,-0.500) (1.0,-0.000) 1.e+30
^^^ ICOAT=7 ^^^^^^^^^^^^^^^^^^^^^^^^^^^^^^^^^^^^^^^^^^^^^^^^^^^^^^^^^^^^^^^^^^^^
--- iboundary
2   <----IBOUNDARY(ICOAT=7)
--- number of layers over air backing
   (1st layer is farthst fr incid field and innermost)
1
--- thick,epsilon(c),mu(c),resistivity(ohm)
3.000 (15.0,-0.500) (1.0,-0.000) 1.e+30



(End of regular input file. Leave a few blank lines)

----------------------------------------------------------------
'OPTIONAL ADVANCE FEATURES' (Do not change letters in quotations)
# The line above must be placed at the end of the regular urbana
```

```
# input. Advance features are designed for special applications or
# for testing codes.  They are not needed by general usages.
# ------------------------------------
# ADVANCE1: ADD GTD-TYPE BLOCKAGE CHECK
# ------------------------------------
# In regular urbana computation, blockage check is mostly done by
# PTD principle. For interior scattering in a confined region, use of
# GTD principle may be more appropriate.
# Option to use GTD principle:  1=yes,    2=no (regular case)
2
# ---------------------------------------
# ADVANCE2: SIMPLE TERRAIN BLOCKAGE MODEL
# ---------------------------------------
# For GO method, terrain generates 100% blockage, and blocked rays leave
# no energy behind a hill.  With this feature, LOS rays and UTD edge
# diffraction rays can pass through terrain, with some attenuation.
# Attenuation is measured in dB per hill.  Each hill is identified
# by two passages through two terrain facets.
# Can only be used with GO method (and UTD edge option).
# Use simple terrain model: 1 = yes, 2 = no (regular case)
2
# Enter coating code range of terrain facets (e.g., 1, 2):
1 1
# Enter amount of attenuation per hill (dB, > 0):
5.
# ---------------------------------------------
# ADVANCE3: APPROXIMATE DOUBLE DIFFRACTION MODEL
# ---------------------------------------------
# For GO + UTD method, only single diffraction is considered.
# With this feature, double diffraction is approximated by identifying
# surfaces which block the single diffraction, such as building walls.
# If one or two facets block the path from the single diffraction point
# to the transmitter, the diffraction is still included, but with attenuation.
# Works best if "diffracting facets", marked by their coating code, are
# always associated with enclosed structures with well defined edges.
# Use double diffraction model: 1 = yes, 2 = no (regular case)
2
# Encounter coating code range of diffracting facets (e.g., 5, 10):
2 2
# Enter amount of attenuation for second diffraction (dB, > 0);
10.
# ----------------------
# ADVANCE4: ACCELERATION
# ----------------------
# For large scenes, run time grows both with the number of field
# observation points and the number of edges.  Normally, all combinations
```

```
# of lit edges and observation points are considered.  This feature
# accelerates the processing by limiting the scope of considered edge
# interactions to region around the LOS path from the transmitter
# to the observation point.  For example, to run a 5 km by 5 km scene,
# one may choose a 250 m interaction radius.  For each observation
# point, edges are ignored that lie outside an ellipse whose foci are the
# Tx and the observation point and whose major axis is the LOS distance
# plus 500 m (radius x 2).
# This feature can also be used to automatically filter edge files
# whose domain far exceeds the domain of observation points.
# Only use this feature for terrestrial simulations where the scene
# is nominally parallel to the x-y plane.
#
# Use large scene acceleration: 1 = yes, 2 = no (regular case)
2
# Enter radius of interaction
250.
# --------------------------
# ADVANCE5: MULTI-DIFFRACTION
# --------------------------
# Substitute for Adv. #3.  Uses ray rubber-banding algorithm to find
# path from transmitter to receiver.
# Can only be used with GO. Cannot be used in conjunction with Adv. #3.
# If UTD switched on above, will take measures not to double count
# single diffraction mechanism.
# Use multi-diffraction model: 1 = yes, 0,2 = no
1
# Enter coating code range of diffracting facets (e.g. 5, 10):
2 2
```

B. FACET FILE FOR 2 HOUSES WITH BARRIER WALL

```
combined facets of two files
8
Combined facet file
0
48
-240.000000 0.000000 132.000000
-240.000000 0.000000 0.000000
-240.000000 -94.332130 0.000000
-240.000000 -94.332130 96.000000
-240.000000 -178.332123 96.000000
-240.000000 -178.332123 0.000000
-240.000000 -240.000000 0.000000
-240.000000 -240.000000 132.000000
168.000000 240.000000 96.000000
```

168.000000 240.000000 36.000000
84.000000 240.000000 36.000000
84.000000 240.000000 96.000000
-241.738739 168.000000 36.000000
-240.000000 240.000000 0.000000
0.000000 240.000000 0.000000
-241.738739 84.000000 36.000000
-241.738739 84.000000 96.000000
-94.332130 240.000000 36.000000
-178.332123 240.000000 36.000000
-178.332123 240.000000 96.000000
-94.332130 240.000000 96.000000
0.000000 240.000000 132.000000
-240.000000 240.000000 132.000000
-241.738739 168.000000 96.000000
240.000000 168.000000 36.000000
240.000000 240.000000 0.000000
240.000000 168.000000 96.000000
240.000000 240.000000 132.000000
240.000000 84.000000 96.000000
-178.332123 -242.335052 36.000000
-94.332130 -242.335052 36.000000
0.000000 -240.000000 0.000000
240.000000 84.000000 36.000000
240.000000 0.000000 0.000000
-178.332123 -242.335052 96.000000
240.000000 -94.332130 36.000000
240.000000 -94.332130 96.000000
240.000000 0.000000 132.000000
-94.332130 -242.335052 96.000000
0.000000 -240.000000 132.000000
240.000000 -178.332123 36.000000
240.000000 -178.332123 96.000000
168.000000 -242.335052 96.000000
240.000000 -240.000000 132.000000
84.000000 -242.335052 96.000000
168.000000 -242.335052 36.000000
240.000000 -240.000000 0.000000
84.000000 -242.335052 36.000000
31
surface
2 3
4 2 3 2 1 1
2 4 1 2 1 2
surface
2 3

5 7 8 2 2 3
7 5 6 2 2 4
surface
2 3
4 8 1 2 3 5
8 4 5 2 3 6
surface
2 3
16 14 2 2 4 7
14 16 13 2 4 8
surface
2 3
2 17 16 2 5 9
17 2 1 2 5 10
surface
2 3
17 23 24 2 6 11
23 17 1 2 6 12
surface
2 3
13 23 14 2 7 13
23 13 24 2 7 14
surface
2 3
31 7 32 2 8 15
7 31 30 2 8 16
surface
2 3
8 30 35 2 9 17
30 8 7 2 9 18
surface
2 3
8 39 40 2 10 19
39 8 35 2 10 20
surface
2 3
32 39 31 2 11 21
39 32 40 2 11 22
surface
2 3
45 32 48 2 12 23
32 45 40 2 12 24
surface
2 3
48 47 46 2 13 25
47 48 32 2 13 26

surface
2 3
43 47 44 2 14 27
47 43 46 2 14 28
surface
2 3
45 44 40 2 15 29
44 45 43 2 15 30
surface
2 3
41 44 47 2 16 31
44 41 42 2 16 32
surface
2 3
44 37 38 2 17 33
37 44 42 2 17 34
surface
2 3
37 34 38 2 18 35
34 37 36 2 18 36
surface
2 3
47 36 41 2 19 37
36 47 34 2 19 38
surface
2 3
38 33 29 2 20 39
33 38 34 2 20 40
surface
2 3
28 29 27 2 21 41
29 28 38 2 21 42
surface
2 3
26 27 25 2 22 43
27 26 28 2 22 44
surface
2 3
26 33 34 2 23 45
33 26 25 2 23 46
surface
2 3
23 21 20 2 24 47
21 23 22 2 24 48
surface
2 3

14 20 19 2 25 49
20 14 23 2 25 50
surface
2 3
14 18 15 2 26 51
18 14 19 2 26 52
surface
2 3
22 18 21 2 27 53
18 22 15 2 27 54
surface
2 3
15 12 11 2 28 55
12 15 22 2 28 56
surface
2 3
26 11 10 2 29 57
11 26 15 2 29 58
surface
2 3
28 10 9 2 30 59
10 28 26 2 30 60
surface
2 3
28 12 22 2 31 61
12 28 9 2 31 62
Combined facet file
0
4
-392.785400 -393.381714 0.985490
391.046631 -393.381714 1.013391
-392.785400 391.046631 0.985485
391.046631 391.046631 1.013390
1
surface
2 3
1 2 4 1 1 63
1 4 3 1 1 64
Combined facet file
0
4
-260.000000 -260.000000 132.000092
260.000000 -260.000000 132.000015
-260.000000 260.000000 131.999985
260.000000 260.000000 131.999969
1

surface
2 3
1 2 4 4 1 65
1 4 3 4 1 66
Combined facet file
0
48
-450.002014 610.000000 132.000000
-450.002014 610.000000 0.000000
-355.669891 609.999207 0.000000
-355.669891 609.999207 96.000000
-271.669891 609.998535 96.000000
-271.669891 609.998535 0.000000
-210.002014 609.997986 0.000000
-210.002014 609.997986 132.000000
-689.998596 1018.002014 96.000000
-689.998596 1018.002014 36.000000
-689.999268 934.002014 36.000000
-689.999268 934.002014 96.000000
-618.002014 608.262695 36.000000
-690.002014 610.002014 0.000000
-690.000000 850.002014 0.000000
-534.002014 608.261963 36.000000
-534.002014 608.261963 96.000000
-690.000793 755.669922 36.000000
-690.001465 671.669922 36.000000
-690.001465 671.669922 96.000000
-690.000793 755.669922 96.000000
-690.000000 850.002014 132.000000
-690.002014 610.002014 132.000000
-618.002014 608.262695 96.000000
-617.997986 1090.001465 36.000000
-689.997986 1090.001953 0.000000
-617.997986 1090.001465 96.000000
-689.997986 1090.001953 132.000000
-533.997986 1090.000732 96.000000
-207.666443 671.665833 36.000000
-207.665741 755.665833 36.000000
-210.000000 849.997986 0.000000
-533.997986 1090.000732 36.000000
-449.997986 1090.000000 0.000000
-207.666443 671.665833 96.000000
-355.665833 1089.999268 36.000000
-355.665833 1089.999268 96.000000
-449.997986 1090.000000 132.000000
-207.665741 755.665833 96.000000

-210.000000 849.997986 132.000000
-271.665863 1089.998535 36.000000
-271.665863 1089.998535 96.000000
-207.663528 1017.997925 96.000000
-209.997986 1089.998047 132.000000
-207.664246 933.997986 96.000000
-207.663528 1017.997925 36.000000
-209.997986 1089.998047 0.000000
-207.664246 933.997986 36.000000
31
surface
2 3
4 2 3 2 1 67
2 4 1 2 1 68
surface
2 3
5 7 8 2 2 69
7 5 6 2 2 70
surface
2 3
4 8 1 2 3 71
8 4 5 2 3 72
surface
2 3
16 14 2 2 4 73
14 16 13 2 4 74
surface
2 3
2 17 16 2 5 75
17 2 1 2 5 76
surface
2 3
17 23 24 2 6 77
23 17 1 2 6 78
surface
2 3
13 23 14 2 7 79
23 13 24 2 7 80
surface
2 3
31 7 32 2 8 81
7 31 30 2 8 82
surface
2 3
8 30 35 2 9 83
30 8 7 2 9 84

surface
2 3
8 39 40 2 10 85
39 8 35 2 10 86
surface
2 3
32 39 31 2 11 87
39 32 40 2 11 88
surface
2 3
45 32 48 2 12 89
32 45 40 2 12 90
surface
2 3
48 47 46 2 13 91
47 48 32 2 13 92
surface
2 3
43 47 44 2 14 93
47 43 46 2 14 94
surface
2 3
45 44 40 2 15 95
44 45 43 2 15 96
surface
2 3
41 44 47 2 16 97
44 41 42 2 16 98
surface
2 3
44 37 38 2 17 99
37 44 42 2 17 100
surface
2 3
37 34 38 2 18 101
34 37 36 2 18 102
surface
2 3
47 36 41 2 19 103
36 47 34 2 19 104
surface
2 3
38 33 29 2 20 105
33 38 34 2 20 106
surface
2 3

28 29 27 2 21 107
29 28 38 2 21 108
surface
2 3
26 27 25 2 22 109
27 26 28 2 22 110
surface
2 3
26 33 34 2 23 111
33 26 25 2 23 112
surface
2 3
23 21 20 2 24 113
21 23 22 2 24 114
surface
2 3
14 20 19 2 25 115
20 14 23 2 25 116
surface
2 3
14 18 15 2 26 117
18 14 19 2 26 118
surface
2 3
22 18 21 2 27 119
18 22 15 2 27 120
surface
2 3
15 12 11 2 28 121
12 15 22 2 28 122
surface
2 3
26 11 10 2 29 123
11 26 15 2 29 124
surface
2 3
28 10 9 2 30 125
10 28 26 2 30 126
surface
2 3
28 12 22 2 31 127
12 28 9 2 31 128
Combined facet file
0
4
-56.621582 457.211273 0.985490

-56.614990 1241.043335 1.013391
-841.049927 457.217896 0.985485
-841.043335 1241.049927 1.013390
1
surface
2 3
1 2 4 1 1 129
1 4 3 1 1 130
Combined facet file
0
4
-190.002197 589.997803 132.000092
-189.997803 1109.997803 132.000015
-710.002197 590.002197 131.999985
-709.997803 1110.002197 131.999969
1
surface
2 3
1 2 4 4 1 131
1 4 3 4 1 132
Combined facet file
0
4
-380.000000 450.000000 0.000000
-20.000000 450.000000 0.000000
-380.000000 450.000000 108.000000
-20.000000 450.000000 108.000000
1
surface
2 3
1 2 4 2 10 133
1 4 3 2 10 134
Combined facet file
0
4
-380.000000 457.375000 0.000000
-20.000000 457.375000 0.000000
-380.000000 457.375000 108.000000
-20.000000 457.375000 108.000000
1
surface
2 3
1 2 4 2 10 135
1 4 3 2 10 136

THIS PAGE INTENTIONALLY LEFT BLANK

LIST OF REFERENCES

[1] P. C. Lui, Lecture notes for DTS 5701, Large Scale Systems Engineering, 2003.

[2] J. B. Andersen, T. S. Rappaport, and S. Yoshida, "Propagation measurements and models for wireless communications channels," *IEEE Commun. Mag*., Vol. 33, No. 1, pp. 42 – 29, January 1995.

[3] J. Walfisch, *UHF/Microwave propagation in urban environments*, Ph.D. dissertation, Polytechnic University, 1986.

[4] J. Walfisch and H. L. Bertoni, "A theoretical model of UHF propagation in urban environments," *IEEE Trans. on Antennas and Propagation*, Vol. 36, pp. 1788 – 1796, December 1988.

[5] R. J. C. Bultitude, P. Melancon, H. Zaghloul, G. Morrison, and M. Prokki, "The dependence of indoor radio channel multipath characteristics on transmit/receive ranges," *IEEE Journal on Selected Areas in Communications*, Vol. 11, No.7, pp. 979 – 990, 1993.

[6] S. Loredo, L. Valle, and R. P. Torres, "Accuracy analysis of GO/UTD radio-channel modeling in indoor scenarios at 1.8 and 2.5 GHz," *IEEE Antennas and Propagation Magazine*, Vol. 43, No. 5, pp. 37 – 51, 2001.

[7] D. C. Jenn, Lecture notes for EC 3630, Radio Wave Propagation, available at www.nps.navy.mil/jenn, 2003.

[8] D. R. J. Chillingworth, G. R. Danesh-Narouie, and Bryan S. Westcott, "On ray-tracing via caustic geometry," *IEEE Antennas and Propagation Magazine*, Vol. 38, No. 5, May 1990.

[9] H. R. Reed and C. M. Russel, *Ultra High Frequency Propagation*, John Wiley and Sons, 1953.

[10] O. Landron, M. J. Feuerstein, and T. S. Rappaport, "In situ microwave reflection coefficient measurements for smooth and rough exterior wall surfaces," *Proceedings IEEE Vehicular Technology Conference*, pp. 77 – 80, May 18 – 20, 1993.

[11] J. B. Keller, "Diffraction by an aperture," *Journal of Applied Physics*, pp. 426 – 444, April 1957.

[12] http://www.bell-labs.com/org/1133/Research/VirtualAcoustics/techno/gtd.html accessed on 11 November 2003.

[13] D. I. Laurenson, *Indoor radio channel propagation modeling by ray tracing techniques*, Ph.D. dissertation, University of Edinburgh, 1994.

[14] P. H. Pathak, "High-frequency techniques for antenna analysis," *Proc. IEEE*, Vol. 80, pp. 44 – 65, 1992.

[15] A. D. Sarma, B. Balakrishna, S. Srikanth, and L. N. Merugu, "Uniform geometrical theory of diffraction for the analysis of on-aircraft antennas. A mini review," *IETE Technology Review*, *15*, pp. 191 – 202, 1998.

[16] P. A. Tirkas, C. M. Wangswick, and C. A. Balanis, "Propagation model for building blockage in satellite mobile communication system," *IEEE Trans. on Antenna and Propagation*, Vol. 46, pp. 991 – 997, 1998.

[17] W. C. Jakes, *Microwave Mobile Communications*, John Wiley and Sons, 1974.

[18] T. S. Rappaport, *Wireless Communications – Principles and Practice*, Prentice Hall, 1996.

[19] J. J. Egli, "Radio propagation above 40 MC/s over irregular terrain," *Proc. IRE*, pp. 1383 – 1391, October 1957.

[20] T. H. de P. Rolim, C. P. D. Novaes, A. de O. Vono, and D. A. Guimarães, "Survey: A system for propagation analysis in mobile communication environments," *INTERTECH Proceedings, VII International Conference on Engineering and Technology Education*, 2002.

[21] F. Ikegami, S. Yoshida, T. Takeuchi, and M. Umehira, "Propagation factors controlling mean field strength on urban streets," *IEEE Trans. on Antennas and Propagation*, Vol. AP – 32, pp. 822 – 829, December 1984.

[22] J. M. Hernando and F. Perez-Fontan, *Introduction to Mobile Communications Engineering*, Artech House, October 1999.

[23] K. Siwiak, *Radiowave Propagation and Antennas for Personal Communications*, Artech House, May 1995.

[24] United States Office of the Secretary of Defense, “Unmanned aerial vehicles roadmap 2002 – 2027,” pp. 33, December 2002.

[25] United States Office of the Secretary of Defence/C3I, “Unmanned aerial vehicles as communications platforms,” pp. 52, November 1997.

[26] http://www.spawar.navy.mil/robots/air/amgsss/mssmp.html accessed on 11 November 2003.

THIS PAGE INTENTIONALLY LEFT BLANK

INITIAL DISTRIBUTION LIST

1. Defense Technical Information Center
   Ft. Belvoir, Virginia

2. Dudley Knox Library
   Naval Postgraduate School
   Monterey, California

3. Professor John P. Powers, Chairman, Code EC
   Department of Electrical and Computer Engineering
   Naval Postgraduate School
   Monterey, California

4. Professor David C. Jenn, Code EC/Jn
   Department of Electrical and Computer Engineering
   Naval Postgraduate School
   Monterey, California

5. Professor Jeffrey B. Knorr, Code EC/Ko
   Department of Electrical and Computer Engineering
   Naval Postgraduate School
   Monterey, California

6. Professor Richard W. Adler, Code EC/Ab
   Department of Electrical and Computer Engineering
   Naval Postgraduate School
   Monterey, California

7. Professor Yeo Tat Soon
   Director
   Temasek Defense Systems Institute
   Block E1, #05 – 05
   Singapore

8. Major Lock Wai Lek Willy
   Singapore